June 2013

# Thermometry using OH laser-induced fluorescence excitation spectra: A feasibility study

Elin Malmqvist

Division of Combustion Physics
Lund University


Master of Science Thesis

**Thermometry using OH laser-induced fluorescence excitation spectra: A feasibility study**



Master thesis in Physics, June 2013

Lund Report on Combustion Physics, LRCP-168
ISRN LUTFD2/TFC - 168 - SE
ISSN 1102-8718

Elin Malmqvist

Division of Combustion Physics Department of Physics
Lund University

P.O. Box 118
S-221 00 Lund
Sweden

**Abstract**

In this thesis, rotational spectra, acquired through laser-induced fluorescence (LIF) on the OH-radical, were used to evaluate temperatures in different combustion environments. By comparing experimental spectra with theoretical ones of known temperature, the temperature can be determined. A MATLAB-code has been developed that evaluates temperature by comparing experimental spectra with a library of theoretical spectra, using a least-square algorithm. The theoretical spectra database was generated with the software LIFBASE. The code was used to evaluate temperature from OH-spectra acquired from already existing excitation scans recorded in an HCCI-engine, using photofragmentation LIF (PF-LIF). The LIF-signal was detected with ICCD-cameras. The measurements are thus spatially resolved in two dimensions. This spatial resolution was utilized to get spatially resolved, quantitative temperature measurements. Some reference excitation scans were performed during this project using both LIF and PF-LIF. These were acquired in premixed, laminar flames and in a free flow of $H_2O_2$-vapor at ambient conditons.

**Acknowledgements**

I would like to thank my supervisors, Joakim Bood and Malin Jonsson, for always taking the time to help and support me during all the stages of this thesis project. A special thanks to Kajsa Larsson for helping me in the lab, and for generously sharing her office with me.

# Contents

# Chapter 1

# Introduction

## 1.1 Background

All human societies have used combustion in some way or form, none as much as our own. It is the dominating energy source in the world and its applications is used for everything from electricity production and heating to industrial production and all forms of transportation [1]. Because of the growing concern about the environment and the climate, it is important to find ways to make combustion as clean and efficient as possible. To achieve this, we must increase our understanding of those factors and properties which control the combustion process. Knowledge of chemical composition is one very crucial property, but temperature also plays a vital role since the two properties are highly dependent [2]. The chemical reaction rate is highly dependent on temperature, which is clearly illustrated by the empirical Arrhenius equation [1],

$$k(T) = Ae^{\frac{-E_a}{R_u T}}, \tag{1.1}$$

where $T$ is the temperature; $k$ is the chemical reaction rate coefficient; $A$ is the pre-exponential factor; $E_a$ is the activation energy; and $R_u$ is the Universal gas constant [1]. Temperature is thus clearly tied to chemical kinetics, but it is also a central factor in pollution, soot formation, energy release rates, and overall combustion effciency. Temperature measurements are particularly central for validating theoretical and numerical combustion models, as well as diagnostic techniques [3]. The advancement of temperature evaluation methods is therefore a crucial component in the developement of new and more efficient engines such as the homogeneous charge compression ignition (HCCI) engine. The aim of this master thesis was to develop a temperature evaluation code, using the programming language MATLAB [4], that is able to generate spatially resolved temperature information from excitation scans on hydroxyl radical (OH). This code was then used to evaluate temperatures from already existing OH-excitation scans recorded in a HCCI engine. The excitation scans evaluated were acquired using laser-induced fluorescence (LIF) and photofragmentation LIF (PF-LIF). OH-LIF is often used for temperature measurements in combustion, because the obtained signal is strong and the measurements can easily be spatially resolved in two dimensions.

The probability of different transitions between energy levels in a molecule

changes with temperature, and in turn, the intensity of the corresponding peaks in an acquired spectrum. Temperature information can thus be obtained by comparing the height and shape of an experimental spectrum with a theoretical spectrum of known temperature. To aquire a spectrum, from which temperature information can be obtained, the energy levels in a molecule have to be probed. In combustion, laser techniques are often used for this, since they are mostly non-intrusive, have single shot potential, and often offer spatial and temporal resolution. Laser based temperature techniques have many advantages over thermocouple probes which are conventionally used for temperature measurement. Thermocouples introduce thermal mass and flow perturbations into the measurement volume, which disturb the chemistry and physics on which the temperature depends. They are also only capable of point measurements [3]. On the other hand, laser techniques are harder to operate and are in general more expensive than thermocouples [5]. Thermocouples are therefore still an indispensable tool for certain temperature measurements both in research and industry.

The developed MATLAB-code compares experimental spectra with theoretical spectra of different temperatures and finds the best fit. The theoretical spectra are simulated in the software LIFBASE [6]. The method of fitting experimental spectra to theoretical ones, is commonly used in thermometry. It is, for instance, regularly applied in temperature measurements with Coherent anti-Stokes Raman Scattering (CARS). For example, Martinsson at al. evaluate temperature by using a least-square algorithm to compare experimental CARS spectra with theoretical spectra [7]. The drawbacks of thermometry with CARS are the complexities of the technique and the fact that it normally only provides point measurements. The online software LIFSIM [8] determines temperature by fitting simulated LIF-spectra to experimental data but this is done on the NO-molecule [8]. Kiefer et al. also use a least-square algorithm to determine temperature [2]. They compare experimental LIF-spectra from OH in flames, with theoretical spectra. This work is very similar to the work that has been done in this thesis. The crucial difference is that now the probed OH-fragments are not naturally occurring OH; they were instead produced through photofragmentation of hydrogen peroxide ($H_2O_2$). These OH-fragments will have a different temperature sensitivity and temperature range than the naturally occurring OH in [2] (see Section 2.8.1).

## 1.2 Main tasks and questions

The main question during the development of the code was: *How can temperature be evaluated from spatially resolved OH-excitation scans?* To find an answer to this question, a number of issues required attention:

- How should the experimental spectra be obtained and prepared before the evaluation?
  - How should potential instrumental broadening be dealt with?
  - How should the wavelength axis be adjusted?
- How should the temperature evaluation be done?

  - What algorithm should be used?
  - How should the spatially resolved evaluation be implemented?
- What are the required inputs and what restrictions do they create?
  - Wavelength interval?
  - Reference pressure and temperature?
  - Saturation regime?
- How should the code be validated?

## 1.3 Outline

The theoretical background is provided in chapter 2. It describes the properties and molecular structure of the OH-radical and the theory behind the applied laser diagnostic techniques. The method section of this report is divided into two parts. The first part of chapter 3 presents the method and material used to carry out the reference measurements. This section also summarizes the engine measurements, by Li et al. [9]. The development of the key parts of the code is described in the second part of chapter 3. Chapter 4 consists of results and discussion and chapter 5 contains conclusion and future outlook.

# Chapter 2

# Theoretical background

## 2.1 Energy levels in molecules

Molecular energy-level structure is considerably more complicated than the structure in atoms, since molecules can vibrate and rotate. Each electronic energy state is split into different vibrational and rotational energy-levels. As seen in Fig. 2.1, the energy difference between electronic states is generally a couple of electron volts (eV), which corresponds to UV-, visible- and near IR-radiation. This splitting is around one order of magnitude greater than the splitting of vibrational levels ($\approx 0.1$ eV) and three orders of magnitude greater than rotational splitting ($\approx 10^{-3}$ eV). Vibrational and rotational splitting corresponds to the IR- and far-IR/microwave-region, respectively [10].

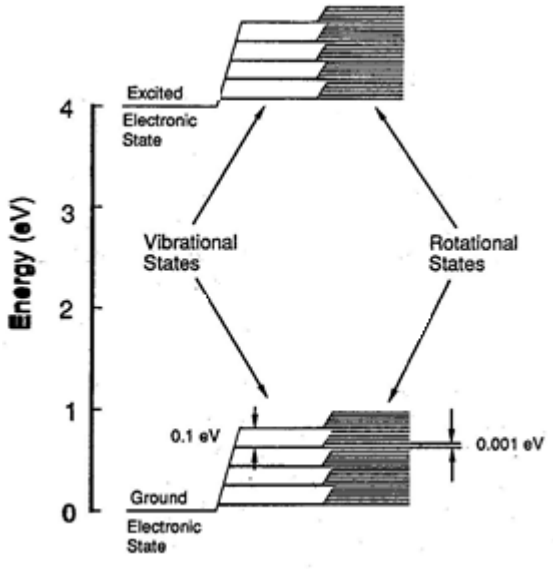


Figure 2.1: Schematic energy levels in a molecule. Each electronic energy level is split up into vibrational levels, which in turn are split into rotational levels. The figure was taken from [10].

## 2.2 Broadening of Spectral Lines

A spectral transition, or spectral line, will always have a finite width. A state always has a finite lifetime, $\Delta t$, which means that it will have an uncertainty in its energy, $\Delta E$, according to Eq. 2.1, the Heisenberg Uncertainty Principle [5],

$$\Delta E \Delta t \geq \frac{\hbar}{2}, \tag{2.1}$$

where $\hbar$ is Planck's constant. This broadening is called the natural line width of a spectral line. The natural broadening is small compared to Doppler and collisional broadening [5].

Doppler broadening dominates at low pressures. It is caused by the thermal motion of molecules. Radiation from molecules moving towards a detector will appear to have a higher frequency and the radiation from those moving away will appear to have a lower frequency. The measured spectral line is thus broadened. A Doppler broadened spectral line has a Gaussian profile (Eq. 2.2) [11],

$$g(x) = A * e^{-(\frac{x-B}{2C^2})^2}, \tag{2.2}$$

for real constant $A$, $B$, $C$. The full width at half maximum (FWHM) of a Doppler broadened spectral line is given by

$$\Delta\nu_D = 2C\sqrt{\ln 2} = \frac{2\nu_0}{c}\sqrt{\frac{2\ln 2 \cdot kT}{m}}, \tag{2.3}$$

where $k$ is Boltzmann′s constant; $T$, the temperature; $m$, molecular mass; $\nu_0$, transition center frequency; and $c$ is the speed of light. Doppler broadening is called inhomogeneous broadening since the shift causing the broadening is not the same for all molecules [5].

Collisional broadening is dominant at high pressures. It is caused by interactions between different molecules. When molecules collide their interaction with radiation is interrupted which leads to a line broadening. Collisional broadening is called homogeneous broadening because statistically all the molecules will contribute equally to the broadening. The profile of a collisional broadened spectral line has a Lorentzian profile [5].

Instrumental broadening is caused by the finite and limited nature of the measurement equipment. Some causes of instrumental broadening are non-ideal optics, resolution and particular method of detection, and the finite size of slits and apertures [12]. Since instrumental broadening is caused by a combination of different phenomenon, it gives a line profile which is partly Gaussian and partly Lorentzian, called a Voight profile. The greatest contribution to the instrumental broadening in this project, is the finite spatial, temporal, and most importantly, spectral profile of the laser. This profile has a Gaussian shape.

## 2.3 Temperature and molecules

Statistical mechanics derives the macroscopic properties of a system from the microscopic properties of the many atoms and molecules that make up the system [13]. Motion is a microscopic property, which means that each individual particle has a specific motion. Temperature, on the other hand, is a macroscopic property; one cannot speak of the temperature of one molecule. Instead,

temperature is the result of the motion, or kinetic energy, of all the particles in a system. The kinetic energy of a molecule involves both internal and external energy modes. Internal energy is a result of electronic, vibrational and rotational motion while external energy arises from the translational motion of the molecule. If the average external or internal energy of a system is changed, so is its temperature [14].

### 2.3.1 Boltzmann equation and population distribution

From a quantum-mechanical point of view, a change in internal energy of a molecule means a change in what discrete rotational, vibrational or electronic energy state it populates. According to statistical mechanics, the population distribution of an ensemble of molecules in thermal equilibrium is given by the Boltzmann equation (Eq. 2.4). It describes the fraction of the total population expected to populate each energy level:

$$P = \frac{N_i}{N} = \frac{g_i e^{-\frac{E_i}{kT}}}{\sum g_i e^{-\frac{E_j}{kT}}}, \tag{2.4}$$

where $N_i$ is the number density of particles in the $i$th state of energy $E_i$; $N$, the total number density; $k$, Boltzmann's constant; $T$, the equilibrium temperature; and $g_i$, the degeneracy factor of state $i$ [5]. Eq. 2.4 clearly shows the strong temperature dependence of the population distribution over the allowed energy states. At low temperatures, most of the molecules will be in the ground energy state, while high temperatures will lead to an increase in the probability of finding molecules at higher energy levels [14]. The Boltzmann equation is only valid for systems in thermal equilibrium, which means that the translational, electronic, vibrational and rotational modes are equilibrated [5]. From a temperature perspective this simply means that their respective Boltzmann distribution indicates the same temperature. An isolated system will always reach thermal equilibrium, given sufficient time [15]. Rotational equilibrium is established after a few collisions between molecules and vibrational equilibrium is reached after a few hundred collisions. At conditions relevant in this project, non-equilibrium effects will rapidly decline and become negligible. For rotational and vibrational energy distributions this takes on the order of 1 and 100 ns, respectively [5].

If a system is not in thermal equilibrium, the population distribution is dependent on more factors than temperature. For instance, after an interaction, molecules might gain extra internal energy and thereby change the population distribution. A different population distribution would complicate temperature evaluation with spectroscopic techniques.

### 2.3.2 Measurement techniques

When the temperature of a system changes, the population distribution will be altered, and this, in turn, means that the probability of the transitions between energy levels will change. Temperature information about a system can therefore be obtained by probing the rotational, vibrational or electronic energy transitions of the molecules with some kind of spectroscopic technique [5]. There are a number of different techniques for measuring temperature. In the

laser diagnostics community, they are usually divided into two groups: those with a coherent signal and those with an incoherent signal. Examples of coherent techniques are CARS and degenerate four wave mixing (DFWM). The coherent techniques typically have a superior signal to noise ratio, but they are experimentally quite complex and are often only carried out in a point. The incoherent techniques, e.g. Rayleight scattering and LIF are more sensitive to background noise but they are usually easier to operate and understand theoretically. It is also quite easy to obtain spatially resolve experiments with them [3].

## 2.4 Fluorescence

The emission of radiation from atoms or molecules that spontaneously relax to a lower energy level (of the same spin multiplicity as the higher level) is called fluorescence. Fluorescence is emitted in all directions. The radiation often originates from another, usually lower, energy state than the level to which the molecules were originally excited. This phenomenon is due to vibrational and rotational energy transfer in the upper state, produced by collisions. If the flourescence signal, obtained from an upper molecular state, was spectrally resolve, a spectrum with many wavelength would be obtained, even though only one transition from the lower state is pumped [5], [16].

There are numerous optical and collisional processes, which increase or decrease the spontaneous emission and thereby affect the amount of fluorescence attained from a specific energy level structure. Fig. 2.2 shows a simplified system, with two energy levels, where these basic physical processes are illustrated.

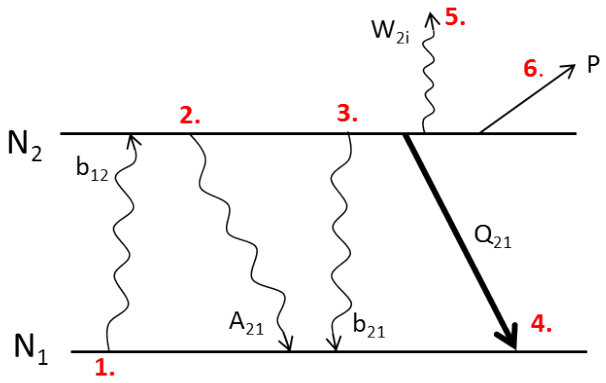


Figure 2.2: The basic physical processes affecting the fluorescence rate shown in a simplified two-level system. The processes are marked with their rate constants, where $b_{12}$ and $b_{21}$ are the stimulated absorption and emission rate constants; $A_{21}$ is the spontaneous emission rate constant; $Q_{21}$ is the quenching rate constant; $W_{2i}$ is the photoionization rate constant; and $P$ is the predissociation rate constant.

For spontaneous emission to occur, the molecule must first be in an excited state. Excitation can happen in a variety of ways, for example through absorp-

tion of photons (1 in Fig. 2.2). After a finite time the molecule might relax into the lower level through spontaneous emission/fluorescence (2). A competing process is stimulated emission (3), in which an incoming photon stimulates an exited molecule to relax and emit a photon with the same energy, phase, polarization and direction as the incident photon. As mentioned above, collisions with molecules in its surroundings may cause a molecule to leave the excited state without emitting radiation, thus decreasing the amount of spontaneous emisson. This phenomenon is called collisional quenching (4). The collisional quenching rate is very high for species at room temperature and pressure. Two additional processes that increase the loss rate from the excited state are photoionization (5) and predissociation (6). The photoionization is a process in which a photon, with large enough energy, ionizes the molecule, and predissociation takes place when a molecule is transferred from a bound state to an unbound (dissociative) state and dissociation occurs [5], [16].

## 2.5 Lasers

The first laser, the ruby laser, was developed in the 1950s and 1960s [10]. Lasers are light sources that can emit highly monochromatic, spatially and/or temporally coherent light through the processes of stimulated emission and optical amplification in a gain medium. This is also what the word laser, which is an acronym of "Light Amplification by Stimulated Emission of Radiation", describes.

Today, there are many different kinds of lasers, but they all contain three basic elements; a gain medium, a means of excitation, and an optical cavity of some sort [5], see Fig. 2.3. The gain medium must allow transitions between energy levels corresponding to the desired wavelength of the laser. For lasing to occur between two energy levels in the gain medium, stimulated emission must dominate over absorption and spontaneous emission. This is achieved by creating a higher population in the upper energy level than in the lower level, a so-called population inversion [10]. At thermal equilibrium, population inversion is impossible to achieve in a two-level system, instead a three or four-level system must be pumped in some manner [5]. A common way is to optically pump it with flash lamps or another laser.

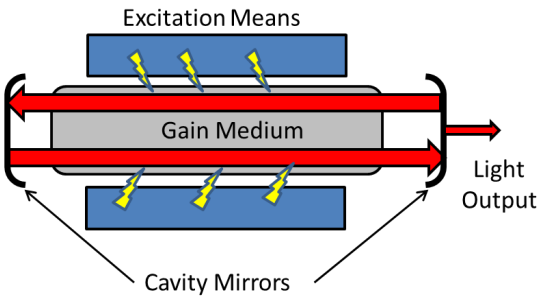


Figure 2.3: A schematic image of a laser cavity. The laser light propagates between the cavity mirrors, through the gain medium, and is amplified. A small part of the light escapes through one of the mirrors and becomes the laser beam.

The lasing process is started by a single photon, created through spontaneous emission, which stimulates electrons to deexcite and emit photons. This emission is not enough to obtain laser light, though. The third component, the optical cavity, is needed for amplification. It is placed around the gain medium, with highly reflective mirrors at each end. The photons from the stimulated emission will propagate back and forth in the cavity and increase the number of stimulated photons. If the gain of one roundtrip in the cavity is greater than the losses, the light is amplified. A laser can have one or several modes that fulfill the gain requirement. A single mode laser has very monochromatic light while a multimode laser does not. One of the mirrors in the cavity has lower reflectivity and let some light escape. The escaped light makes up the laser beam [5]. The spectral purity, coherence and power have made the laser an invaluable tool in a multitude of research areas and applications, including spectroscopy.

### 2.5.1 Nd:YAG and Dye Lasers

The two types of lasers used in this project are Nd:YAG lasers and dye lasers. The active medium in an Nd:YAG-laser, is trivalent neodymium ions, $Nd^{3+}$, housed in a yttrium aluminum garnet crystalline host material ($Y_3Al_5O_{12}$) [5]. The Nd:YAG laser is a pulsed, four-level laser normally pumped by flash lamps. The most commonly used lasing transition gives radiation with a wavelength of 1064 nm; see Fig. 2.4 for schematic representation [10].

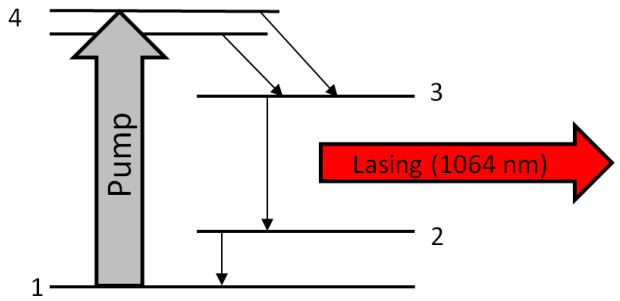


Figure 2.4: In the four-level system, the atoms are pumped from a long-lived level (1) to an upper level that has a very short lifetime (4). The atoms instantly decay to a long-lived level (3). Lasing occurs through stimulated emission between level 3 and 2. The level where the atoms end up after lasing (2) is very short-lived and the molecules immediately decay down to the first level (1) and the process starts again [10].

The Nd:YAG laser emits certain fixed frequencies, determined by the atomic energy states in the Nd-ions. A molecular system has many more available energy states, as a result of its vibration-rotational structure. Lasers with a molecular active medium thus provide a greater number of frequencies. Complex organic molecules in solution, called dyes, possess a very large number of closely packed vibrational-rotational energy levels. The energy levels are broadened by interaction and collisions with surrounding molecules and form

continuous energy bands. This means that the radiation from a dye laser can be continuously tuned over a wide frequency range, which size depend on the specific dye ($\approx 10$ nm). Dye lasers are usually radiation pumped, either by flash lamps or another laser [5]. In this thesis project, the dye laser used was pumped by an Nd:YAG laser.

## 2.6 Laser-induced fluorescence (LIF)

Lasers provide a very convenient method of achieving spatially, temporally and spectrally selective excitation. Laser-induced fluorescence is a spectroscopic technique, in which laser radiation is absorbed by the studied species and the resulting fluorescence is typically detected perpendicular to the direction of the laser beam [5]. It is one of the most commonly used techniques in combustion diagnostics [2]. It is relatively simple to operate and allows detection of minor species and volatile radicals in low concentration [3], at ppm or even sub-ppm levels [5]. Many radicals and pollutants, which are important for combustion, are present in this concentration range. Another advantage of using LIF is that disruptive stray laser light often easily can be filtered away because fluorescence typically has a longer wavelength than the laser radiation [5], [16]. Furthermore, LIF can easily be spatially resolved in two dimensions by forming the laser beam into a sheet and detect the fluorescence signal with a camera. Many combustion intermediates have therefore been detected by LIF [5].

### 2.6.1 LIF-spectra

There are two different ways of recording LIF-spectra. The laser can be tuned to a specific absorption line while a spectrometer detects the fluorescence, spectrally resolved. The fluorescence spectrum yields information about the population distribution of the upper state since it is the spectral distribution of the fluorescence that is monitored. Alternatively, an excitation scan can be performed, where the laser is scanned across various absorption lines and the total fluorescence is monitored. In principle, an excitation scan yields the absorption spectrum and provides information about the population distribution of the lower state [5]. It would be possible to obtain information about the upper state during a excitation scan by using a narrow filter to select spectral information from the detected fluorescence signal [5].

### 2.6.2 LIF-signal

LIF can only be used on atoms or molecules that fluoresce which means that they must have accessible bound states. These state must also be accessible with a laser. To be able to perform quantitative LIF measurements, the emission spectrum of the molecule and the rate of radiative decay of its excited state must be known. Losses from the excited state, due to non-radiative processes, such as collisional quenching and predissociation, must also be accounted for [5]. This was discussed in section 2.4.

If photoionization and predissociation are negligible in a simplified two-level system (see Fig. 2.2), the signal intensity is proportional to the rate of spontaneous emission from the upper state ($N_2A_{21}$). It may be expressed as

$$I_{LIF} \propto \nu_{21} l N_2 A_{21} = \nu_{21} l N_1^0 \frac{B_{12}}{B_{12} + B_{21}} \frac{A_{21}}{1 + \frac{I_{sat}^{\nu}}{I_{laser}}}, \tag{2.5}$$

where $A_{21}$ is the spontaneous emission rate constant. $B_{12}$ and $B_{21}$ are the Einstein coefficient for stimulated absorption and emission. The parameter $\nu_{21}$ is the frequency of the fluorescence photons, $l$ is the measurement volume length, $N_1^0$ is the initial ground state populated number density of the absorbing species, $I_{laser}$ is the laser intensity, $I_{sat}^{\nu}$ saturation spectral intensity [2], [5]. For a more detailed description of the fluorescence signal expression see [5].

### 2.6.3 Linear regime

For low laser intensity ($I_{laser} << I_{sat}^{\nu}$) expression 2.5 reduces to

$$I_{LIF} \propto \nu_{21} l N_1^0 A_{21} I_{laser} \frac{B_{12}}{A_{21} + Q_{21}}. \tag{2.6}$$

The number of signal photons is linearly proportional to the number of laser photons delivered during a pulse. This is called the linear regime. The intensity of the LIF-signal is dependent on the quenching rate, $Q_{21}$, and the spontaneous emission rate constant, $A_{21}$. Consequently, the quenching rate must be evaluated to be able to make quantitative concentration measurement in the linear regime. Since $Q_{21} >> A_{21}$ at normal temperatures and pressures, the efficiency is much smaller than unity and the fluorescence signal, obtained in the linear regime, is therefore relatively weak [5].

### 2.6.4 Saturated regime

For high laser intensity ($I_{laser} >> I_{sat}^{\nu}$) the intensity of the fluorescence signal can be described by

$$I_{LIF} \propto \nu_{21} l N_1^0 A_{21} \frac{B_{12}}{B_{12} + B_{21}}. \tag{2.7}$$

The fluorescence signal is independent of both laser intensity and quenching. The absorption and stimulated emission rates to and from of the upper level are so large that they dominate over all other energy transfers in the upper state. This is called the saturated regime. In this regime, quenching does not have to be considered. The fluorescence signal is maximized at full saturation, which means that maximized detection is obtained. However, it is very difficult to achieve complete saturation. The power in the wings of the focused laser is always low, which makes full spatial saturation virtually impossible to achieve. The laser also varies throughout the duration of a pulse, so temporal saturation is also very difficult to accomplish [5]. Figure 2.5 illustrates a laser energy dependence plot for the fluorescence signal. The linear and saturated regimes are marked.

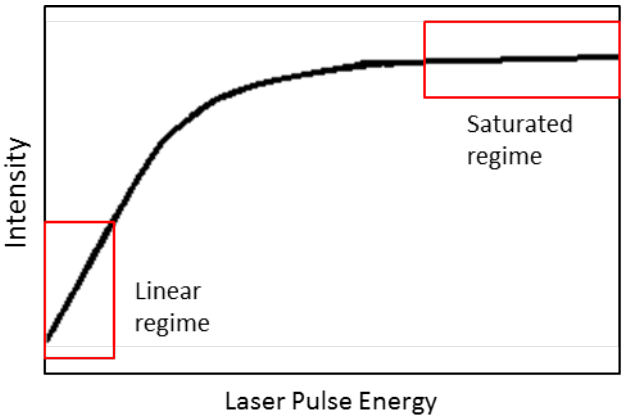


Figure 2.5: A schematic figure of the LIF-signal dependence on laser energy. At low pulse energies the signal is in the linear regime. Here the intensity of the signal is low. The signal intensity is at its highest in the saturated regime, where it does not increase with increasing laser energy.

## 2.7 The hydroxyl radical (OH)

In this thesis, LIF-techniques have been applied to the OH-radical. The OH-radical is a very important species in combustion chemistry since it plays a vital role in the oxidation of hydrocarbon fuels. The great advantage of detecting the OH-radical in hydrocarbon combustion is that it is present in relatively high concentrations. The high concentration produces sufficient signal intensity for single-shot planar measurement which is needed in turbulent environments [3]. OH can also be found in a wide area of flames and it has a relatively high equilibrium concentration compared to other radicals like HCO or CH. This means that OH is frequently used as a flame marker, but it is employed in more novel diagnostic techniques as well [2]. An additional advantage of OH is that it has a high absorption cross section at energies correspondig to the wavelength of many conventional lasers with high pulse intensity. OH is therefore probably the best studied flame intermediate in the combustion community.

Temperature measurements utilizing OH have been performed in numerous ways. Prior to the invention of the laser, OH-thermometry was done with classical emission and absorption spectroscopy. These days, absorption-based laser techniques or coherent laser techniques are used e.g. conventional absorption spectroscopy, cavity ring-down absorption spectroscopy, and polarization spectroscopy. One of the most common methods for determination of OH temperatures is LIF [2].

### 2.7.1 OH-LIF

As mentioned previously, the energy gap between vibrational levels are much smaller than for electronic levels. Excitation of pure vibrational upper levels in most flame radicals and minor pollutants requires tunable infrared radiation [5]. This is also true for the OH-radical which is problematic since tunable IR-radiation is not widely available from a single source [5]. On the other

hand, the transition between the electronic ground state ($X^2\Pi$) and the first excited state ($A^2\Sigma^+$) in OH is around 300 nm [16] which is a wavelength region conveniently accessed by tunable dye lasers [16]. This fact, combined with the high fluorescence signal caused by the high concentration of OH, makes LIF a very attractive method for measuring OH in hydrocarbon combustion. Furthermore, the rotational distribution of OH appears in a relatively narrow frequency interval, but the individual lines are well separated and do not strongly interfere with each other. This means that the spectrum can be highly resolved [2].

#### 2.7.1.1 OH-Structure

The electronic transition ($A^2\Sigma^+ \leftarrow X^2\Pi$) is the most commonly used in LIF measurements on OH. Fig. 2.6 is a edited version of a figure in [16] and it is a schematic illustration of this transition. The molecules will be excited from a rotational level, $i$, in the vibrational ground state ($\nu'' = 0$) of $X^2\Pi$ to rotational level, $j$, in either the ground ($\nu' = 0$) or the first excited ($\nu' = 1$) vibrational level in $A^2\Sigma^+$. These are the transitions with highest transition strength since it decreases rapidly with increasing $\nu'$. In addition to this, higher vibrational levels in $A^2\Sigma^+$ ($\nu' > 1$) have much greater predissociation rates because of the three unbound states that cross it. One of those unbound states, $^4\Sigma^-$, is drawn in Fig. 2.6 and the arrow, P, illustrates how molecules cross over to the unbound state from higher vibrational levels [16]. The measurements used for the temperature evaluation in this project were done using the transition $A^2\Sigma^+(\nu' = 1) \leftarrow X^2\Pi(\nu'' = 0)$, at around 283 nm.

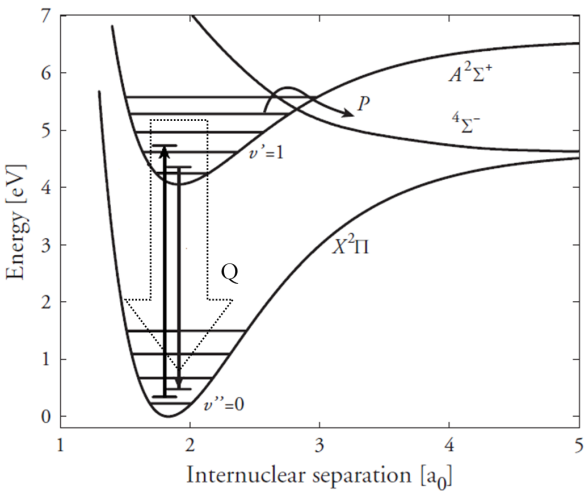


Figure 2.6: The electronic transition $A^2\Sigma^+(\nu' = 1) \leftarrow X^2\Pi(\nu'' = 0)$. The large arrow represent the collisional quenching rate, Q. The arrow is large because this is the dominating deexcitation process at normal pressures [16]

.

Figure 2.7 shows this transition resolved on a rotational level. The ground state has two spin components which give rise to two rotational energy ladders,

due to spin-orbit interaction, starting with $J = 3/2$ and $J = 1/2$. These are termed $F_1$ and $F_2$ respectively. For more information about molecular structure and splitting, the reader is referred to a work on molecular and atomic physics or spectroscopy, e.g. [10],[17]. Hund's coupling case (a) (see Appendix A) is valid for low J-values. There is a strong spin-orbit interaction for the low values, which splits the energy levels into two ladders. This is clearly shown in Fig. 2.7. At high J-levels the spin-orbit interaction becomes weak and the difference between the levels in $F_1$ and $F_2$ becomes small. Hund's coupling case (b) is now a good description of how the angular momenta couples in $X^2\Pi$. When coupling case (b) dominates, the quantum number J is replaced by N. The excited state only has one spin component and, as a result, only one rotational energy ladder. During an excitation scan, the laser is scanned over the rotational levels in the lower electronic state and the fluorescence from the upper state is detected. Each transition will give rise to a peak in the recorded spectrum. The transitions between the rotational levels in $X^2\Pi(\nu'' = 0)$ and those in $A^2\Sigma^+(\nu' = 1)$ create different transition branches [16]. These can be seen in Table 2.1. In Fig. 2.7 the transition $Q_1(5)$ is marked with an arrow. The number in parenthesis describes the N number of the lower level and the subscript indicates between which energy ladders the transition occurs.

Table 2.1: Different transition branches.

| $\Delta$ J | Branch |
|---|---|
| -2 | O |
| -1 | P |
| 0 | Q |
| +1 | R |
| +2 | S |

## 2.8 Photofragmentation laser-induced fluorescence (PF-LIF)

It is not possible to use LIF as a detection technique on all molecules since they might yield low or non-existing fluorescence, due to lack of accessible bound electronic states. This is the case for the important combustion intermediate hydrogen peroxide ($H_2O_2$), when it is excited by UV-radiation. The molecule will not fluoresce after excitation; instead it will dissociate into fragments and yield a continuous featureless absorption spectrum. It can still be detected with fluorescence spectroscopy by probing the resulting OH-fragments with LIF. This technique is called photo-fragmentation LIF (PF-LIF) [9]. It is an indirect technique since it is the fragments and not the parent molecule that are probed. Most of the OH-spectra used for temperature evaluation in this report were obtained through PF-LIF on $H_2O_2$.

PF-LIF can be performed with one laser or with two separate lasers. In this project, PF-LIF was performed with two lasers. A pump laser was set to a wavelength with high cross section for photolysis of the molecule, and a probe laser was scanned over the desired absorption lines of the resulting OH-fragments.

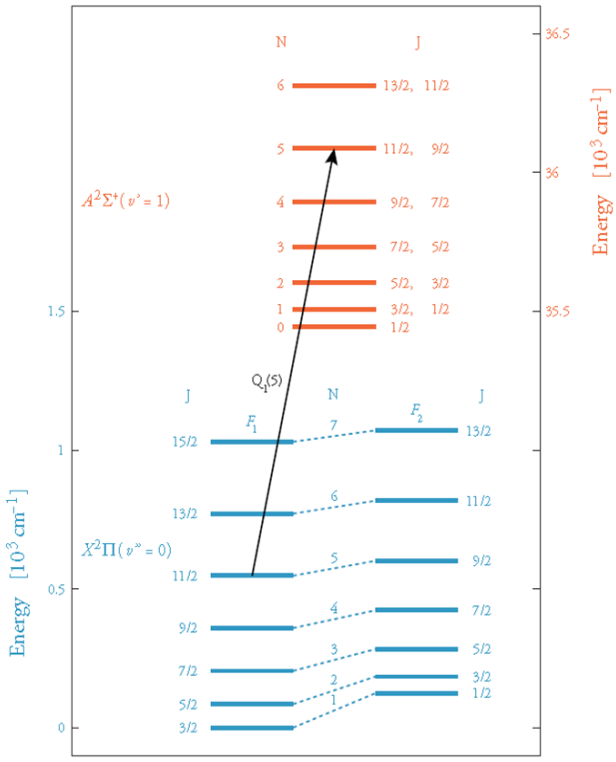


Figure 2.7: The vibrational transition $A^2\Sigma^+(\nu' = 1) \leftarrow X^2\Pi(\nu'' = 0)$ on a rotational level. The lower vibrational state (blue) has two rotational energy ladders, $F_1$ and $F_2$, while the upper vibrational state (red) has one. The rotational transition $Q_1(5)$ is marked with an arrow in the figure. Figure is taken from [16].

Figure 2.8 schematically illustrates PF-LIF on $H_2O_2$.

There must be a certain time-delay between the pump and the probe laser pulse, to ensure that the OH-fragments are in thermal equilibrium and that no unwanted interference induced by the pump pulse disturbs the probing of OH [9]. For PF-LIF experiments carried out on $H_2O_2$-vapor, the LIF-signal has an exponential decay when plotted against the delay time between pump and probe. If the photolysis is weak enough, the chemical consumption of OH is a first order reaction and the LIF-signal follows a single exponential decay [16]. The exponential decay is illustrated in Fig. 2.9, where the signal intensity is plotted at different delay times and a single exponential function has been fitted to the data. To maximize the LIF-signal, the delay time between the lasers should thus be as short as possible since the signal becomes weak fast.

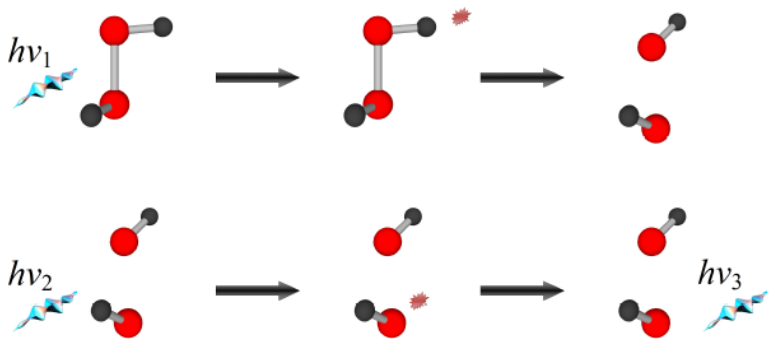


Figure 2.8: A photon from the pump-laser, with frequency $\nu_1$, is absorbed and excites the $H_2O_2$ molecule to an unbound state. The molecules dissociate into OH-fragments. After a certain time delay, a second photon with frequency $\nu_2$, excites the created OH-fragments, which emit fluorescence with frequency $\nu_3$. The figure was taken from [16]

.

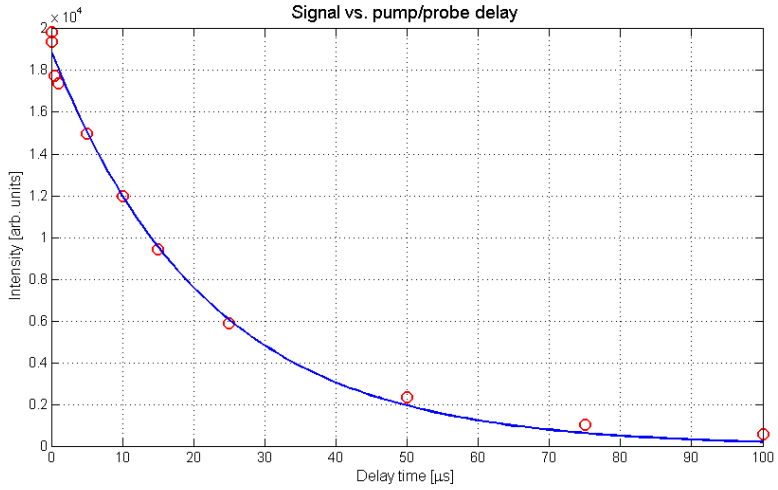


Figure 2.9: Exponential decay of the intensity of the PF-LIF-signal as a function of pump/probe delay time. The measurements were performed on $H_2O_2$-vapor.

### 2.8.1 Temperature measurement with PF-LIF

OH is a radical, which means that it is highly reactive and essentially only exists as an intermediate in reactions. The OH-concentration is therefore very low in combustion before the temperature is high enough for these reactions to start. This is the main drawback of using OH as indicator molecule for temperature; the concentration, and therefore the LIF-signal, drops rapidly with decreasing temperature. Meier et al. suggests that the concentration-decrease is by a factor of 2 each 100 degrees Kelvin, at stoichiometric equilibrium [18]. The accessible temperature range for imaging of OH, is therefore approximately above 1300

K due to the limited signal sensitivity and dynamic range of typical ICCD cameras. This limitation means that it is technically not possible to probe the full probability distribution of temperatures in a combustion process [18]. A solution to this problem is PF-LIF. PF-LIF applied on $H_2O_2$, produces OH-fragments at the same temperature as the original environment. OH can thus be used to probe temperatures in a larger temperature range - even at low temperatures where the chemical production of OH is very low.

The fact that OH can be probed at lower temperatures generates an additional advantage since the temperature dynamics of OH is much stronger at lower temperatures and the temperature measurement should therefore be more accurate. This temperature sensitivity can be explained by looking at the Maxwell-Boltzmann statistics of OH. The fractional population on rotational level J in ladder $F_i$ is given by Eq. 2.8 [16].

$$\frac{N_i}{N} = \frac{g_J e^{-\frac{E(J)}{kT}}}{\sum g_m e^{-\frac{E_{F_1}(m)}{kT}} + \sum g_n e^{-\frac{E_{F_2}(n)}{kT}}} \tag{2.8}$$

In Fig. 2.10, O. Johansson has used the expression in Eq. 2.8 to plot the fractional populations of rotational level $J = 3/2, 7/2, 11/2$ in the $F_1$ branch as a function of temperature [16]. For low temperatures, the slopes of the fractional population curves are steep which means that there is high temperature dependence. As temperature increases the curves become more and more flat and the change in population becomes less and less temperature dependent. The temperature sensitivity of a molecule depends on the structure of its energy levels.

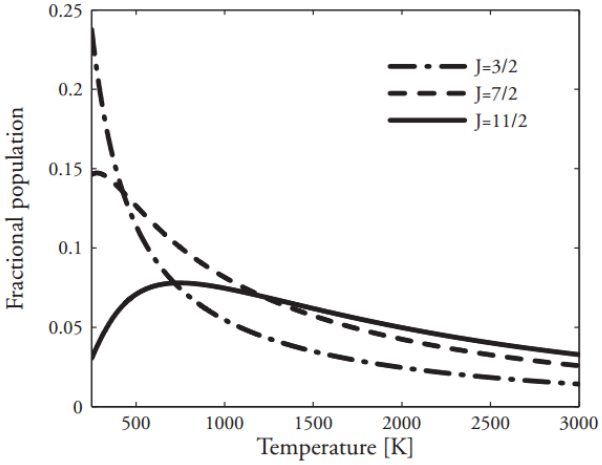


Figure 2.10: The temperature sensitivity of OH-populations in rotational level J = 3/2, 7/2 and 11/2 in the $F_2$-ladder.

# Chapter 3

# Method

The procedure used to develop a means for temperature evaluation can be divided into a few key stages. These are:

- Development of the MATLAB code and creating theoretical spectra database.
- Evaluate temperature from theoretical LIFBASE spectra.
- Perform measurements in laboratory to obtain reference spectra in flames and vaporized $H_2O_2$.
- Try the code on reference spectra.
- Try the code on engine data.
- Implement spatial resolution on data from experiments on vaporized $H_2O_2$.
- Implement spatial resolution on engine data.

The first part of chaper 3 describes the procedure of obtaining reference spectra in the laboratory. The second part describes the development and implementation of the MATLAB code and the theoretical spectra database.

## 3.1 Reference Experiments

To be able to test the code, OH-excitation scans were carried out in environments of known temperature and pressure. LIF and PF-LIF were used to measure OH in laboratory flames and in a $H_2O_2$-vapor created by a bubbler.

### 3.1.1 ICCD-Camera

All the excitation scans used in this thesis were recorded by gated ICCD cameras. They can detect a spatially resolved signal and they have high sensitivity, low dark current and a large dynamic range. ICCD stands for intensifed charge coupled device. A CCD is a semiconductor detector divided into many light sensitive pixels, arranged in a two-dimensional array. When a photon hits a pixel it is converted into one electron at the most, through the photoelectric effect. These electrons are collected in potential wells in each pixel and the amount of

electrons is measured at the end of the collection time [5]. The number of electrons is directly proportional to the intensity of the incident light on each pixel. The stored charge that makes up the image is then digitalized and transferred to a computer. An ICCD camera is a CCD-camera with an image intensifier mounted in front of it. The intensifier amplifies the light before it hits the CCD screen. The intensifier is also needed effciently gate a CCD camera.

During all the excitation scans done for this project, fluorescence from OH was collected and detected perpendicular to the propagation direction of the laser beam. An excitation scan detected with an ICCD camera is made up of many frames taken while the laser is scanned. A typical image from an ICCD camera can be seen in Fig. 3.1. The image depicts the OH-signal in a premixed propane/air flame where the laser is tuned on the transition $R_2(10)$, at 281.87 nm. In this flame, the OH concentration is very low in the unburned zone, the preheat zone and the reaction zone. In principle, OH only exists in the product zone, where the temperature has become high enough for the reactions that produce OH to occur [16]. This concept is clearly illustrated in Fig. 3.1 where the OH-signal is essentially zero outside the product zone.

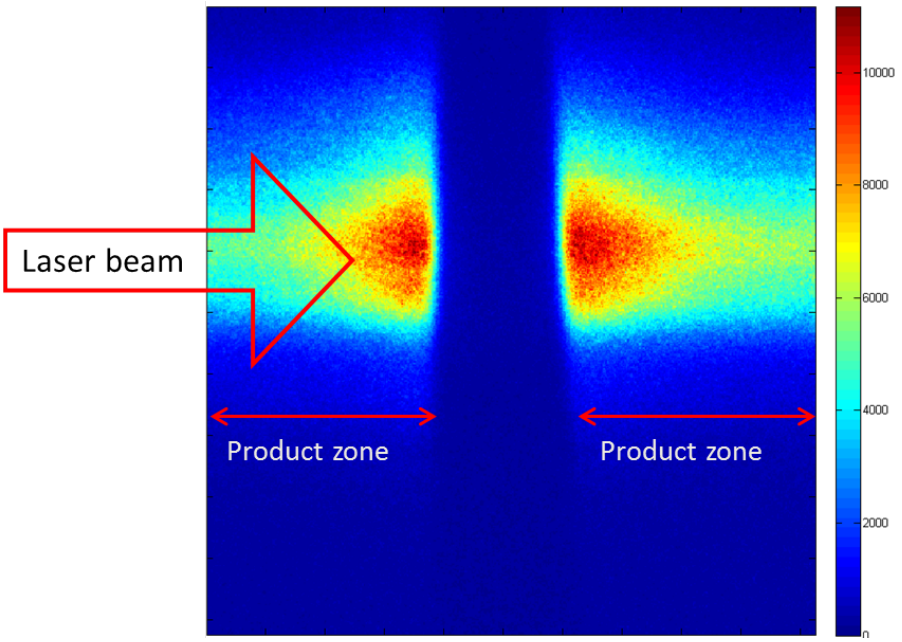


Figure 3.1: An image of the OH LIF-signal in a propane/air flame of stoichiometric mixture, collected with an ICCD camera. The image is taken perpendicular to the propagation direction of the laser beam.

### 3.1.2 LIF measurements in Flames

Excitation scans on naturally occurring OH were performed in premixed, laminar flames using LIF. The flames were a methane/air flame and a propane/air flame at stoichiometric mixture ($\phi = 1$). The burner used was a coaxial burner. For more specifics on the coaxial burner see [19]. The temperature in the product zone of these flames should be around 2200 K. The experimental setup is

presented in Fig. 3.2. Three excitation scans, with a width of 0.5 nm, were performed with a frequency doubled dye-laser, pumped by the second harmonic of an Nd:YAG laser. The scans were carried out with a speed of 0.002 nm/s and together they covered the wavelength range 281.5-283 nm. The dye used in the laser was Rhodamine 6G dissolved in ethanol, with an emission peak at around 560-670 nm [20]. The pulse repetition rate of the laser was 10 Hz and the pulse duration was about 5 ns. The UG11 Schott filter in Fig. 3.2, supresses the 532 nm light from the pump laser, and lets the frequency doubled 283 nm light through.

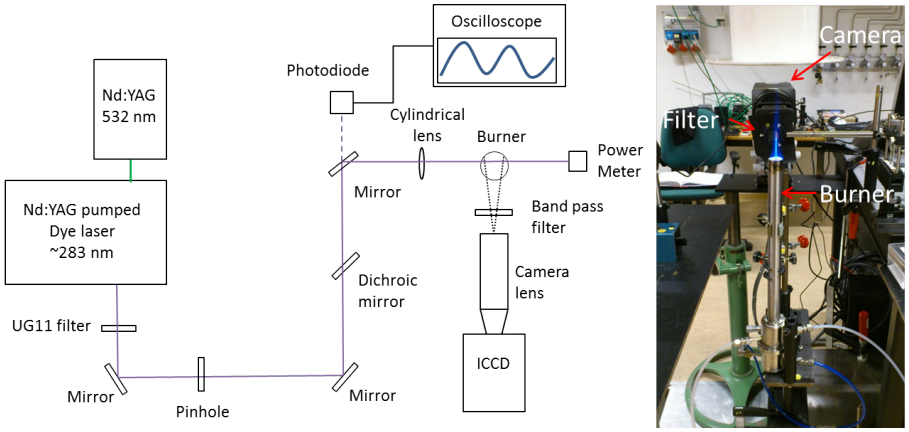


Figure 3.2: The experimental setup for the excitation scans in the flames can be seen to the left. On the right side there is a picture of the coaxial burner.

The beam was shaped into a vertical sheet by a cylindrical lens before it was focused in the center of the flame. The detection was done with an ICCD camera (Princeton Instruments, PIMAX2), with 512x512 pixels, and 450 frames were recorded per scan. Each frame is made up of 10 exposures, which means that they are an accumulation of the fluorescence signal from 10 laser pulses. A band pass filter (centered at 320 nm) was placed in front of the camera to remove interfering light such as stray light from the laser. The camera had a UV-objective connected to it, mounted on a bellow. Background images were also taken with 10 accumulated exposures. One with only the flame, one with only the laser, and one with everything turned off (dark current). There is always a peak at which a dye gives the greatest laser energy output, so when the laser is scanned the output energy changes. If longer scans are carried out there will be a substantial difference in laser intensity across the acquired spectrum. The change in laser energy must be compensated for in some way. The laser energy was therefore measured with a photodiode connected to an oscilloscope. A first degree polynomial was fitted to the energy data and the acquired spectrum was then divided by it.

A power dependence study was performed on the LIF-signal in the methane flame, to check if there were problems with saturation. This study was done by tuning the laser to a transition in OH where the signal is high and measuring the signal intensity for different laser energies (0.18-3.4 mJ). At each pulse-energy, four images were taken with 10 exposures, and the average intensity was plotted against pulse energy, see Fig. 3.3. The laser energy was measured

with a power meter behind the burner. It was discovered that the pulse energy used in the methane flame ($\approx 0.9$ mJ) was outside the linear regime. The linear regime merely seems to extend to slightly below 0.5 mJ. The pulse energy was therefore lowered when the measurements in the propane flame were carried out. The attenuation was done by using UV-filters.

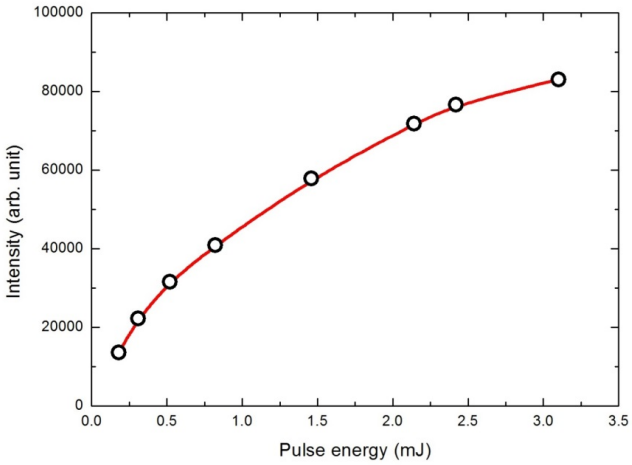


Figure 3.3: Power dependence of the LIF-signal intensity. The linear regime seems to occur approximately between 0 and 0.5 mJ.

### 3.1.3 PF-LIF Measurements in $H_2O_2$-vapor

Excitation scans on OH were acquired with PF-LIF on $H_2O_2$. The measurements were carried out at room temperature and atmospheric pressure. The experimental setup is shown in Fig. 3.4. It is very similar to the setup used for the measurements in the flames, described in in Section 3.1.2. The burner was replaced by a bubbler. The bubbler is a flask containing a liquid $H_2O/H_2O_2$ mixture (50/50 wt-%). Nitrogen is continuously injected into the solution to create vaporized $H_2O_2$. OH-fragments created by PF-LIF on $H_2O_2$ are detected above the opening of the bubbler flask.

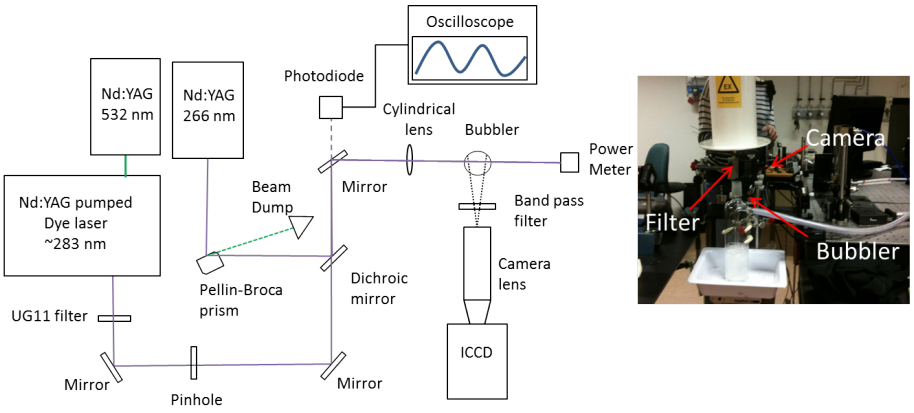


Figure 3.4: The experimental setup for the excitation scans with PF-LIF in $H_2O_2$-vapor can be seen to the left. To the right, there is a photo of the bubbler and accessories.

Two separate laser beams were used to perform PF-LIF on $H_2O_2$. The OH-fragments were probed with the same dye laser as described in the previous section (section 3.1.2). The pump laser, used for photolysis of $H_2O_2$ into two OH-fragments, was a 266 nm-beam from an Nd:YAG laser, equipped with a fourth harmonic frequency conversion unit. The laser generates two overlapping beams at 266 nm and at 532 nm. These were separated with a Pellin-Broca prism and the 532 nm beam was trapped in a beam dump. The pump and probe beams were spatially overlapped by using a dichroic mirror which has high transmittance for the probe beam (283 nm) and high reflectance for the pump beam (266 nm). The detection was done with a ICCD camera (Princeton Instruments, PIMAX-3) with 1024x1024 pixels. The scans consist of 3500 frames with 10 exposures per frame, and it covers the wavelength range 281.1-284.3 nm. A Schott WG 305 filter was placed in front of the camera to remove interfering light. A dark current image, for background, was also taken with 10 exposures. The laser energy was once again measured with an oscilloscope to be able to compensate for changes in intensity in the spectrum. This compensation was even more important during these scans since they were around 3 nm long and would extend over a great part of the gain profile of the dye.

Two excitation scans were performed. During the second scan the energy of the probe beam was reduced to avoid saturation. The delay time between the q-switch and the flash lamps in the pump beam for the dye laser was increased. This method might decreases the quality of the laser profile, so it is vital to make sure it still looks good.

### 3.1.4 Engine Measurements

The reason for measuring $H_2O_2$ in engines is that it is a crucial intermediate in fuel-oxidation chemistry. Reactions involving the production and consumption of $H_2O_2$ are vital for the autoignition process. For example, thermal decomposition of $H_2O_2$ plays an important part in diesel engine ignition and it is of importance for engine knock in spark ignition engines. $H_2O_2$ is especially important in a homogeneous charge compression ignition (HCCI) engine, since its

operation is dependent on simultaneous autoignition at multiple locations which is controlled by the decomposition of $H_2O_2$ into two OH radicals [9], [21].

Li et al. have measured spatially resolved mean $H_2O_2$-concentration at different crank angle degrees (CADs) in a HCCI engine using PF-LIF [9]. When the piston in an engine is at its highest point, called top dead center, it is at 0 CAD and 360 CADs equals one revolution of the piston. The experimental set up, in the engine measurements, was very similar to the one described in Section 3.1.3. They also used a pump-probe strategy for photolyzing $H_2O_2$, and detecting the OH-fragments. The probe laser was tuned to the $Q_1(6)$ transition and 100 single shots were accumulated at each CAD. The optical access to the engine was provided by a cylinder extension in quartz. This kind of concentration measurement provides vital information for modelers and engine-designers who are trying to better understand and control autoignition in HCCI-engines.

Figure 3.5 was taken from the results of reference [9]. The red line represents the OH signal when both lasers are fired (PF-LIF). This signal comes from both naturally occuring OH and OH-fragments created with PF-LIF on $H_2O_2$. The blue line with triangles is the signal when only the probe laser is on and is hitting a resonance in OH (OH-LIF). This signal should come from OH which were not created by photofragmentation. The green line is the background signal of OH-LIF. The probe laser is tuned off an OH absorption line. The black line is obtained by removing the contribution of natural OH (2) from the total OH-signal (1). Hence, the black line represents OH that was created through photofragmentation of $H_2O_2$ (and $HO_2$). Theoretical models predict no chemically produced OH at CADs below -5 CAD since the temperature is not high enough. The fact that there is such a signal (blue line with circles) at those CADs, is most likely due to a weak photolysis caused by the probe laser. For more details on the engine and the engine measurements see [9].

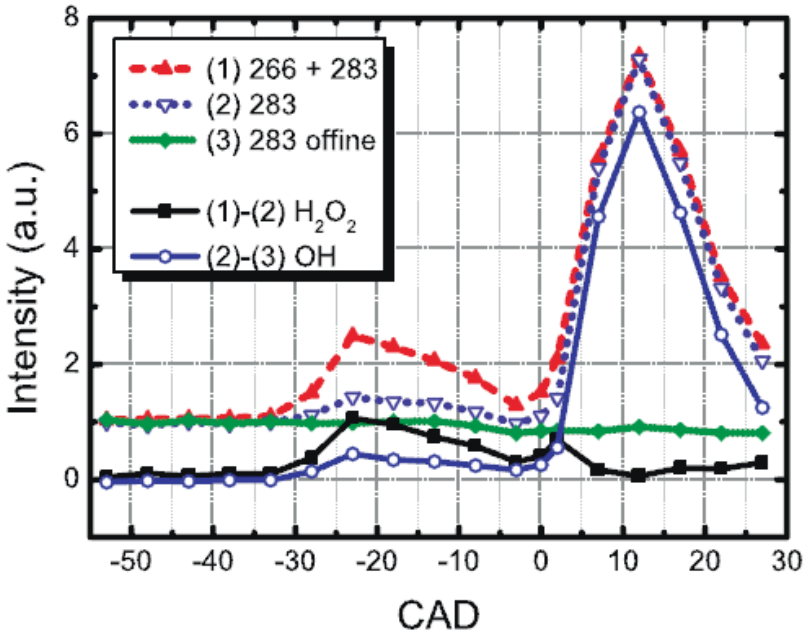


Figure 3.5: Measured OH-signal in a HCCI-engine at different CADs. The red line represents the signal from both natural occuring OH and OH-photofragment. The blue line with triangles represents the signal from OH which was not produced through photofragmentation by the 266 nm-beam. The green line is background of OH-LIF. The black line comes from OH-fragments produced through 266 nm photolysis of $H_2O_2$. The contribution from natural ocuring OH has been removed. The blue line with circles reprents the final OH-LIF signal when background has been removed [9]

Li et al. also performed PF-LIF excitation scans at specific CADs to verify that the measured signal indeed originated from OH [9]. When the excitation scans were performed, the laser was synchronized with the engine speed in such a way that there was a laser pulse fired at the exact same CAD in each engine cycle. The scans are thus taken over many engine cycles while the laser is scanned. The excitation scans were recorded with both the probe and pump beams on, and therefore measure both naturally occuring OH and OH-photofragments. The major goal of developing a code that evaluates temperatures from OH-excitation scans was to be able to obtain spatially resolved temperature measurements from these engine scans. This kind of data would provide further essential information for those studying and simulating autoignition. The excitation scans used for temperature evaluation in this thesis were acquired at -23 and -13 CAD. Both of these CADs correspond to times prior to autoignition and there should be virtually no naturally occuring OH present. Approximate adiabatic mean temperatures were calculated from mean pressure traces taken during the engine measurements. These pressures and temperatures are referred to as reference pressures and temperatures from now on and are found in Table 3.1. These values were used as input for the temperature evaluation code.

Table 3.1: Calculated mean temperature and pressure in the HCCI-engine

| CAD | Temperature [K] | Pressure [bar] |
|---|---|---|
| -23 | 816 | 15 |
| -13 | 950 | 22 |

## 3.2 MATLAB code

The code preforming the temperature evaluation is written in the programming language MATLAB [4]. The code can be found in Appendix B. It evaluates temperature from experimental spectra by finding the best fit among a set of theoretical spectra of different temperatures collected in a database. The most important input to the program is OH experimental excitation spectra in the region 281.0-284.5 nm. To obtain reliable temperatures from the program these scans have to be acquired in the linear regime. The pressure at which the spectra were taken is also required. The program can also adjust the wavelength-axis to better fit the experimental and theoretical peaks, if this is not done beforehand. The program then requires an approximate temperature. When evaluating the engine scans, the approximate calculated mean temperature was used. Fig. 3.6 shows a flowchart of the main tasks performed by the code during the temperature evaluation. The dotted arrows represent input to the code.

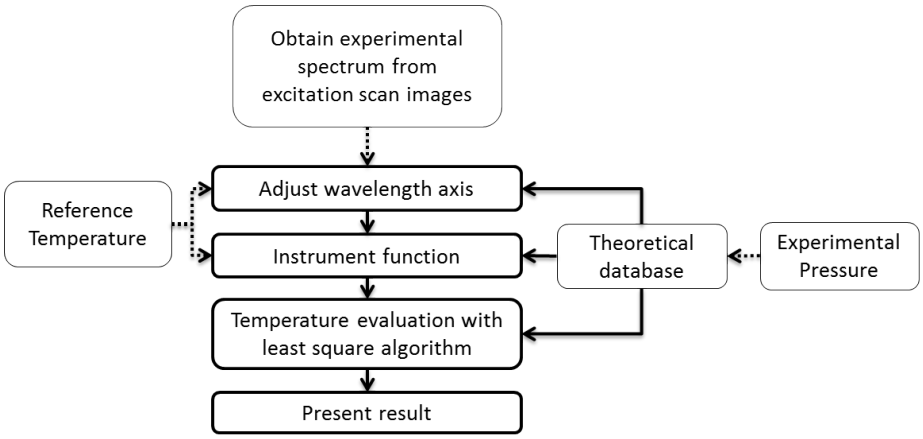


Figure 3.6: Flow chart of the main parts of the MATLAB code. The dotted arrows represent input to the main program.

### 3.2.1 Theoretical data base

A database of theoretical OH excitation spectra was created during this project. At each integer pressure between 1 and 25 bar, there are spectra in the temperature range 200-2300 K. The temperature is changed with steps of 25 K. At certain pressures and temperatures there are also spectra convoluted with different instrumental functions, which are used for determination of the instrumental function. The spectra were simulated using the software LIFBASE [6]. LIFBASE takes into account processes such as predisociation, and differ-

ent line-broadening when calculating spectra. For more information about how LIFBASE simulates LIF spectra see [6].

#### 3.2.1.1 LIFBASE settings

The spectral range of the simulated excitation scans was set to 281.0-284.6 nm in air. The LIF-regime was set to linear and the system was set to thermalized. The FWHM of the instrumental function cannot be set to zero when simulating spectra in LIFBASE. The FWHM was therefore set to a very low value (0.0001 Å), at which it seemed like a decrease in FWHM did not affect the simulated spectrum. See more about the instrumental function in Section 3.2.5.

LIFBASE calculates collisional broadening with the empirical formula,

$$\Delta\nu_{FWHM} = a * P * (\frac{300K}{T})^{b}. \tag{3.1}$$

$P$ is the pressure in bar; $T$, is the temperature in Kelvin; $\Delta\nu_{FWHM}$ is collisional broadening given at full width at half max in $cm^{-1}$; $b$ is a temperature exponent and $a$ is a constant with unit $cm^{-1}$/bar. In the simulation the temperature exponent $b$, were set to 0.8. This constant was taken from measurement presented in [22]. $a$ was calculated to be 0.41 $cm^{-1}$/bar, using the value of $b$ and measurements done by [23] in flames at 2000 K.

### 3.2.2 Preparation of experimental spectrum

The excitation scans are made up of many ICCD images. To obtain a spectrum from these scans, the intensity of the signal from each image is summed up. This value makes up an intensity point in the spectrum at the wavelength the image corresponds to. When this procedure has been done to all the images, a complete spectrum is obtained and information such as temperature can be evaluated from it. Fig. 3.7 illustrates this process on an absorption peak in an OH spectrum. In the figure, the intensities of all the pixels in the image are summed. The process of obtaining spectra from the ICCD-images is different for each scan. No generalized code has been written for this process but the principle is the same for all of them.

- **The background is removed from all the images in a scan.** Background images were taken for the reference scans. Since these scans were taken at atmospheric pressure (1 bar), the baseline where there is no signal was set to zero. There are no background-measurements available for the engine scans and the high pressure causes enough collisional broadening to cause the baseline to be non-zero. In the engine images a part is covered by the piston and a mean value of this intensity was used as a background value.

- **The intensities of all the pixels of interest, in each frame, are summed up to form the intensity values in the spectrum.**

- **Potential start and end defects are dealt with by removing these values.** Examples of these kinds of effects are when the scan ends in the middle of the slope of a peak or if the number of images taken by the camera was not properly synchronized with the laser scan.

- **Create the wavelength axis.** The first and the last point in the spectrum are then assigned their corresponding wavelength values. The wavelength axis between the values is then assumed to be linear. Possible non-linearities will be dealt with in the main program.

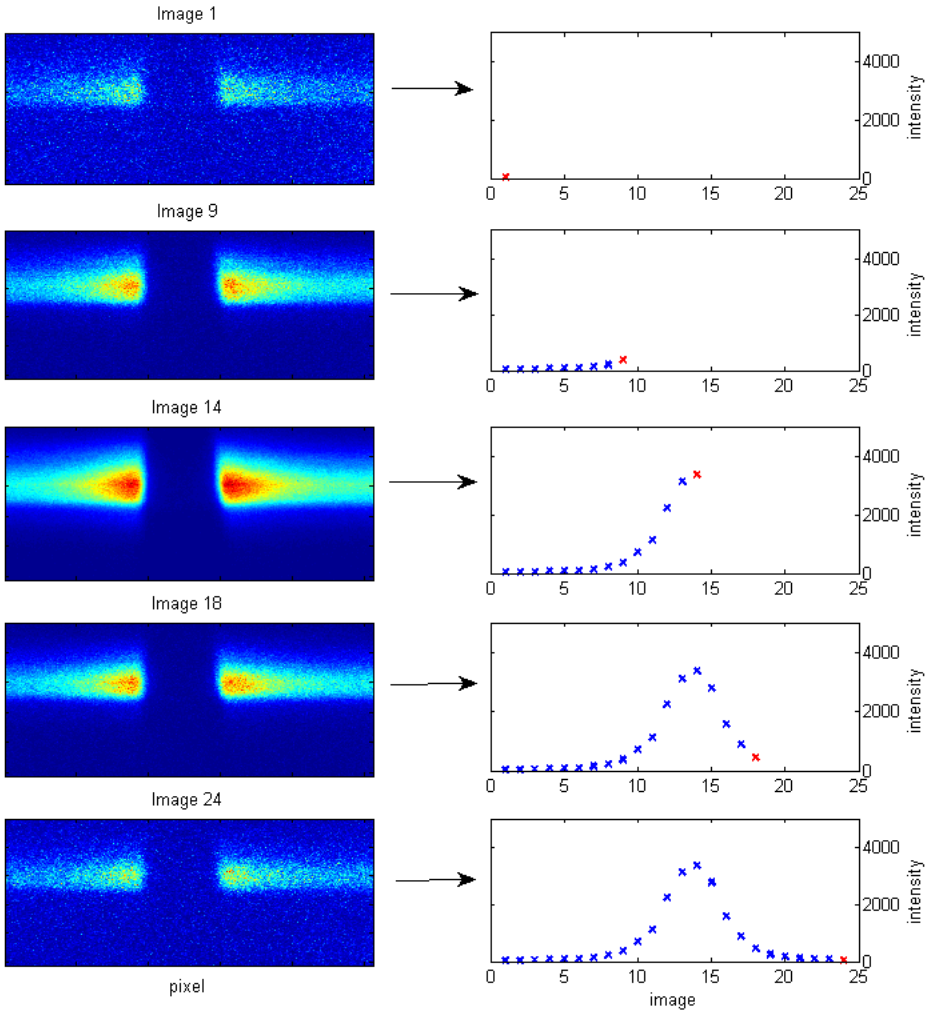


Figure 3.7: Process of obtaining spectrum from excitation scan recorded with an ICCD camera. The intensities in each pixel in an image (at the left) are summed up and become an intensity value in the spectrum at the corresponding wavelength (at the right).

### 3.2.3 Wavelength axis

As mentioned in Section 3.2.2, experimental excitation scans usually do not have a perfectly linear wavelength axis. To be able to compare experimental spectra with theoretical ones this non-linearity must be dealt with. This is done by fitting selected peaks with their theoretical values and the polynomial obtained in the fit is used to adjust the wavelength axis. For the flame measurements the theoretical peaks were selected manually. For the other scans a function was written which requires experimental pressure and a reference temperature as input. It finds peaks in the theoretical spectrum, which match the given temperature and pressure, and then it finds and fits them with the corresponding experimental peaks. The polynomial correcting the wavelength scale is calculated once with the intensity of the whole signal as reference.

### 3.2.4 Least square method

The experimental spectrum is compared with all the theoretical spectra for the specific input pressure to find the theoretical temperature with the best fit. Before they can be compared, the theoretical spectra are convoluted with the previously determined instrumental function. As seen in Eq. 3.2, both the theoretical and experimental spectra are normalized (length of vector = 1). It is thus the spectral shape and not the temperature dependent intensity that is fitted [7]. The fit is done with a least-square algorithm, see Eq. 3.2. The algorithm calculates the residual between the experimental and theoretical spectrum, in each point. The temperature is then obtained by interpolating and minimizing the sum of squares (SSQ) difference corresponding to all the different theoretical spectra (different temperatures).

$$SSQ = \sum_{i=1}^{N} \left( \frac{I_{th}(\lambda_i)}{\sqrt{\sum_{k=1}^{N} I_{th}^2(\lambda_k)}} - \frac{I_{ex}(\lambda_i)}{\sqrt{\sum_{k=1}^{N} I_{ex}^2(\lambda_k)}} \right)^2 \tag{3.2}$$

Where N is the number of pixels in experimental spectrum; $\lambda_i$, the wavelength at pixel $i$; $I_{ex}$, experimental intensity; $I_{th}$, theoretical intensity. The fit is not weighted which means that all the pixels contribute equally to the SSQ [7].

#### 3.2.4.1 Engine scans

There are no background measurements available for the engine scans which could be the reason for the offset that is observed when engine spectra are compared with theoretical spectra at the approximate temperature. This offset causes problems when the temperature is evaluated from the spatial resolved data becasue it is not the same for all the pixel rows. One way to deal with this offset is to adjust the experimental spectrum, in some way. Before the experimental spectrum is compared with each theoretical spectrum it is adjusted so one of its valleys fits with the same valley in the the theoretical spectrum. Temperature evaluation was carried out on the engine excitation scans both with and without this adjustment.

### 3.2.5 Instrumental function

The instrumental function describes the instrumental broadening of the spectral lines. As mentioned in Section 2.2, it is caused by many different properties and it has normally a Voight profile. No specific measurements were done to measure the slit function or laser profile during the measurements, so the instrumental function was approximated as a Gaussian because of the dominating Gaussian laser profile. It is defined as the FWHM (in Å) of a Gaussian profile, see Eq. 2.2.

Ideally, an excitation scan at atmospheric pressure and known temperature would be carried out with the measurement setup and the resulting excitation spectrum would be used to determine the instrumental function. This procedure was done for the reference scans in the flames and in the $H_2O_2$-vapor since the pressures and temperatures were well known. To estimate the instrumental function, a least square algorithm (see Section 3.2.4) was used. The peak $P_1(2)$, in the experimental spectrum was compared to the theoretical peak simulated with different instrumental functions and the best fit was found. The theoretical spectra were simulated at the input reference pressure and temperature.

The temperature and pressure during the engine scans are not well known and no reference scan was taken at known pressure and temperature. The calculated mean temperature from the pressure traces could possibly be used as reference when the instrumental function is approximated. Unfortunately, the above mentioned offset of the engine data made it very hard to use the least square algorithm to find the instrumental function. The instrumental function was instead approximated by manually fitting the spectra with theoretical spectra at the reference temperature and pressure in LIFBASE and finding the instrumental function that gives the smallest residual.

### 3.2.6 Spatial resolution

Theoretically, it is possible to extract a spectrum from each pixel in the image and in this way evaluate temperature pixel by pixel. Spatially resolved temperature evaluation of the OH-signal was done on the data from the PF-LIF measurements performed in the engine and in $H_2O_2$-vapor . The images were resolved in the x and the y directions separately. A spectrum was created from each pixel row in the image and a temperature was evaluated from it. Because the signal was weaker for the scan in $H_2O_2$-vapor, they were evaluated with a some sort of moving average where the intensity of both the previous and subsequent row were included. This averaging technique smooths some of the variations caused by low signal, but it also decreases the spatial resolution somewhat.

The start and end of the pixel rows evaluated were decided by inspecting the quality of the resulting spectra. The evaluated intervals for the two excitation scans recorded in $H_2O_2$-vapor can be seen in Fig. 3.8. The interval of evaluated pixel-rows in the y-axis was different for the different CADs. In Figure 3.9, these intervals are shown on an image from the engine scans. The range of the scan at -13 CAD is smaller because the piston is cutting off a part of the laser sheet and hence the LIF-signal. As seen in Fig. 3.5, the PF-LIF signal in the engine is lower at -13 CAD than at -23 CAD which results in an even smaller spatial range in which good spectra are obtained. The lower intensity makes the

spectra more sensitive to noise, and this fact combined with possible increase of the chemical reactions caused by higher pressure and temperature make the spectra from -13 CAD noisier.

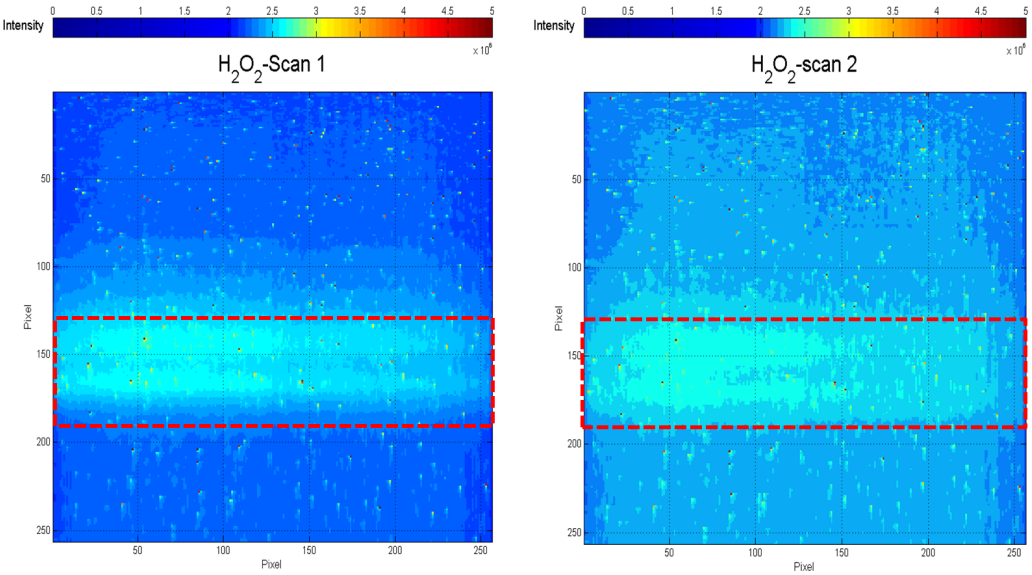


Figure 3.8: The signal from all 3500 intensity images in the excitation scans performed in $H_2O_2$-vapor are accumulated and the ranges of the spatial temperature evaluation are marked with the red line. The left image, corresponding to a scan, was taken with higher laser pulse energy and is thus more saturated. During the second scan (right image) the pulse energy was lowered to decrease saturation effects.

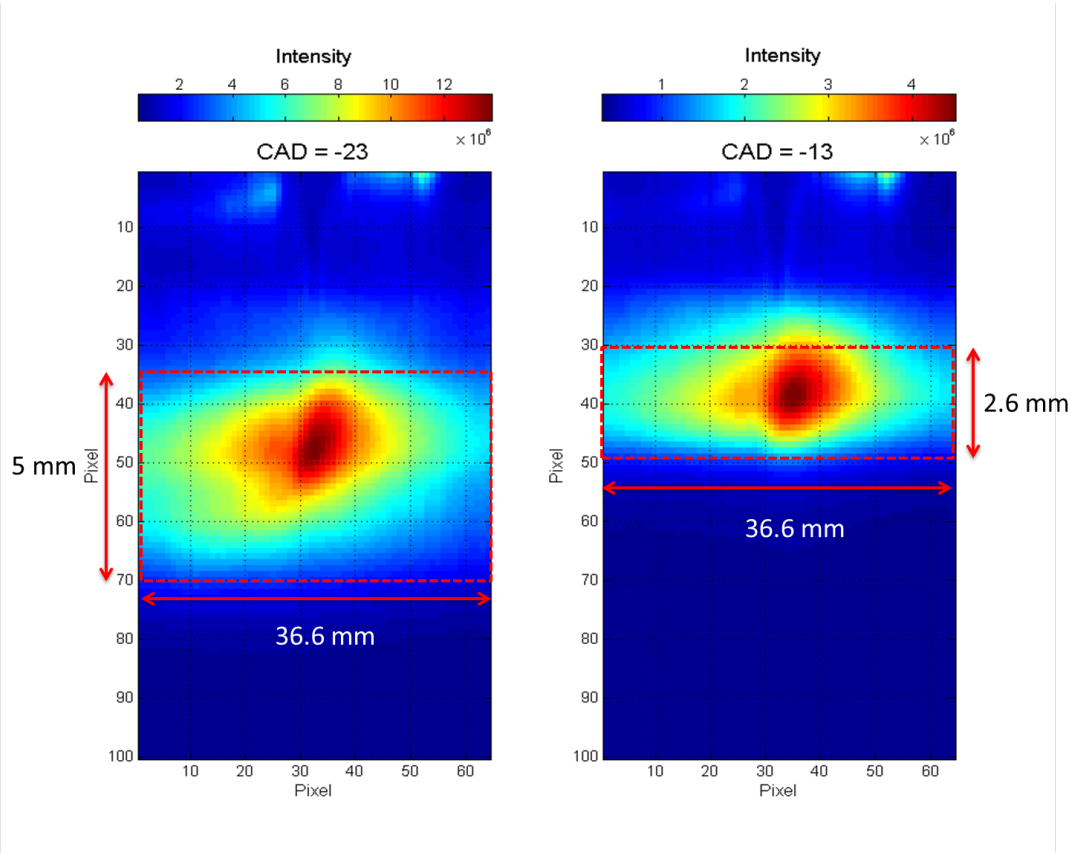


Figure 3.9: The signal from all 2200 intensity images in the excitation scans, at -23 CAD (left) and -13 CAD (right), acquired in the engine are accumulated and the ranges of the spatial temperature evaluation are marked with dashed red lines. The signal that can be seen in the upper part of the image is reflection and scattering on the metallic inlet and exhaust valves in the engine. The dark blue area at the lower part of the images corresponds to an area covered by the piston. At -23 CAD the piston is lower than at -13 CAD, where it cuts off part of the signal. The approximate length of the evaluated areas are represented with arrows in the two images.

# Chapter 4

# Results and discussion

## 4.1 Evaluation of theoretical spectra

As an initial test for the evaluation algorithm, spectra simulated with LIFBASE were used as input. Fig. 4.1 and 4.2 display some of the results. Fig. 4.1 shows the results from the temperature evaluation with the least square method for spectra at 1, 6, and 15 bar. The evaluated temperatures were 300, 700, 1100 and 1500 K. Fig. 4.2 displays the evaluation of four spectra at random, increasing temperatures, at 1 bar. The theoretical spectra all had the wavelength range 281.0-284.6 nm and an instrumental function with a FWHM close to zero (0.0001 Å). The evaluated temperatures correspond well to the theoretical temperatures. They are a little off for some of the spectra at 1 bar which is probably due to an issue with LIFBASE that was discovered during the temperature evaluation. For some spectra there is a sudden discontinuity in the sum of squares curve at around 700 K. This issue is evident in Fig. 4.3, where the absolute values of the approximate derivative ($\frac{\Delta y}{\Delta x}$) of the results in Fig. 4.2 are plotted. To make sure that there was not something in the code causing the discontinuety, spectra were manually compared in LIFBASE, and at temperatures around 700 K the residual suddenly increase considerably when the temperauture is changed 0.1 K.

To investigate this problem further, spectra convoluted with different instrumental functions were evaluated and their SSQ-plots and their derivatives are shown in Fig. 4.4 and Fig. 4.5, respectively. The temperature and pressure in Fig. 4.4 was 434 K and 1 bar. The peculiar "discontinuity effect" is very substantial for small instrumental functions but less so for increasing FWHM. When one inspects the derivative, there seem to be similar, but smaller, effects at other temperatures as well. Fig. 4.5 displays the same information as in Fig. 4.4, but at 15 bar instead. The effect is not observable on these curves. The problem only seem to be prominent at small instrumental broadenings and at low pressure which indicates that the issue is connected to the implementation of the instrumental function in LIFBASE and it should have an insignificant effect on the temperature evaluation at higher pressures.

Temperature evaluation at small instrumental broadenings tend to give greater errors. This error could possibly be due to the discontinuity-effect, but also the fact that the spectra in the database cannot be simulated without instrumental

broadening. For decreasing pressure and FWHM of the instrumental function, there will be an increasing contribution from this small additional instrumental broadening during the convolution done in the LSQ-algorithm.

The temperature sensitivity of OH-spectra, discussed in Section 2.8.1, is quite obvious in the above mentioned SSQ-plots. At low temperatures the slopes of the curves are very steep while they level out for higher temperatures. If the derivative of a curve is greater, the exact minimum point that determines the temperature, can be identified with higher accuracy.

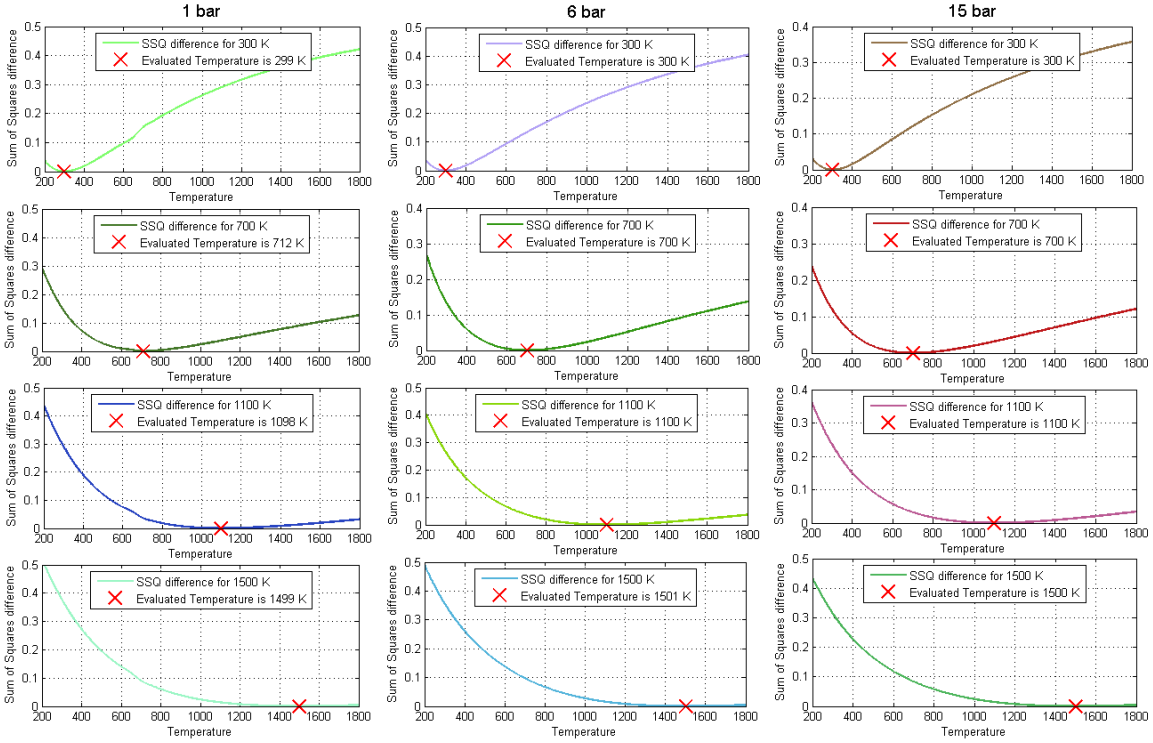


Figure 4.1: Sum of squares (SSQ) plots for theoretical spectra, at different pressures (1, 6, 15 bar) and temperature (300, 700, 1100, 1500 K). Minimized sum of squares difference, which represent the evaluated temperatures, is marked with a red X in each plot. Theoretical and evaluated temperature can be seen in the legend bar at the top of each plot.

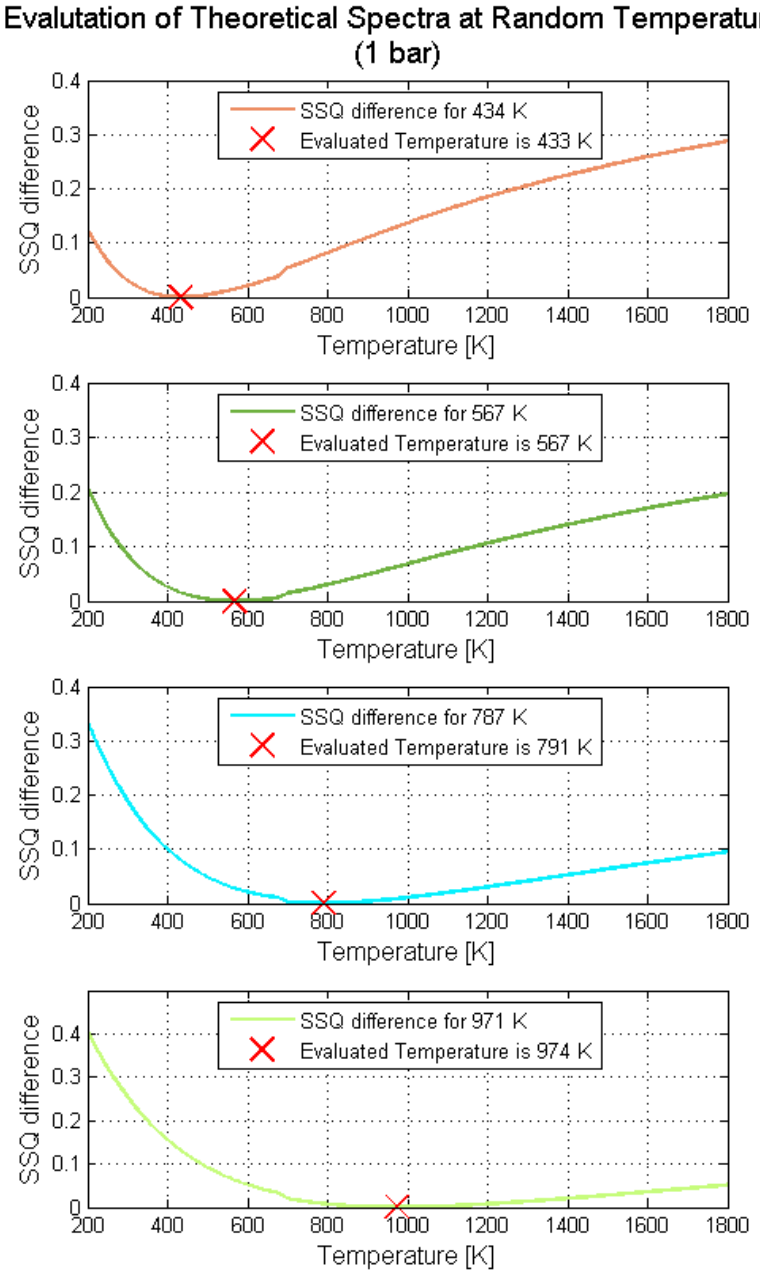


Figure 4.2: Sum of square plots for theoretical spectra at different temperatures (434, 567, 787, 974 K) at 1 bar. Minimized SSQ difference is marked with a red X. Theoretical and evaluated temperature can be seen in the legend bar at the top of each plot.

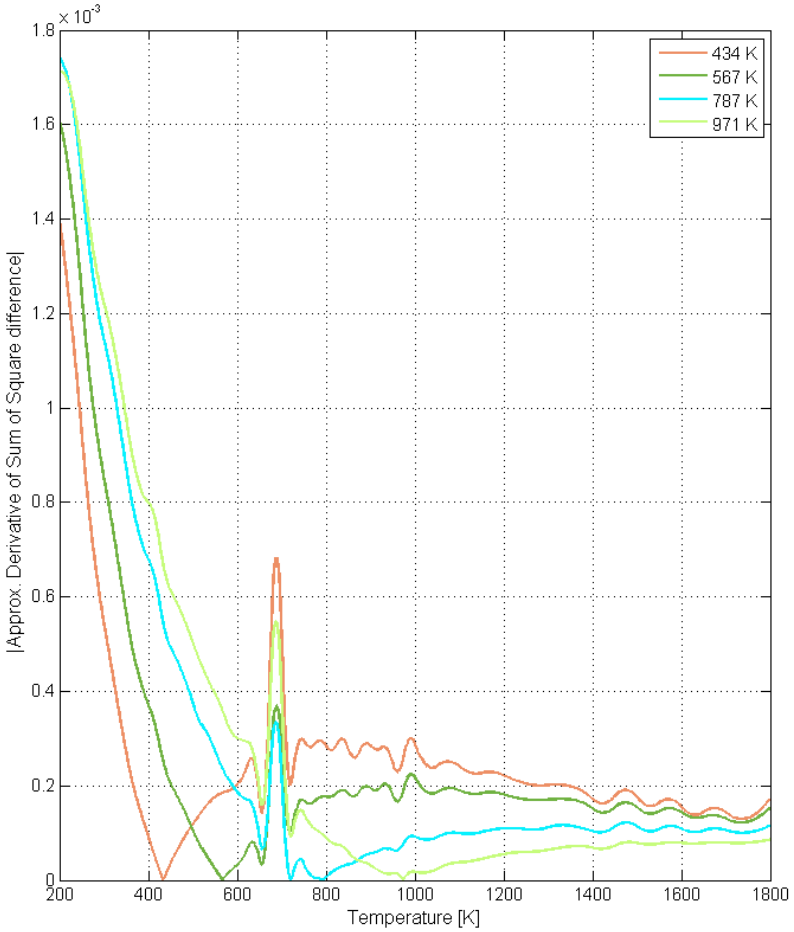


Figure 4.3: Approximate derivative of the sum of squares difference, for the spectra evaluated in Fig. 4.2. The discontinuity at around 700 K is very clear in the plots.

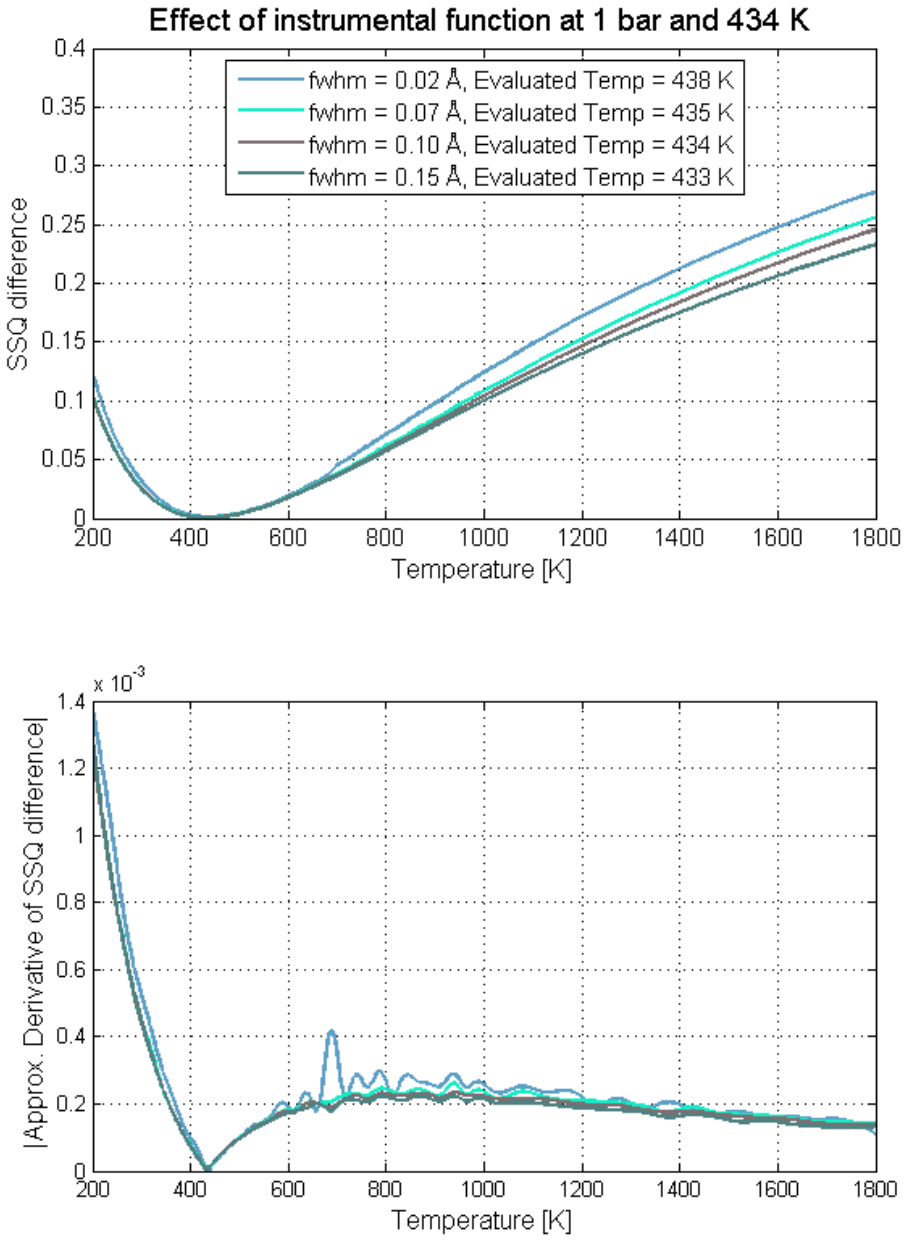


Figure 4.4: Spectra at 1 bar and 434 K evaluated with different different FWHM (0.02 Å, 0.07, 0.10, 0.15 Å) of the instrumental function. In the top diagram the, SSQ-plot can be seen. The result of the minimization for each FWHM can be seen in the legend bar at the top of the plot. The bottom plot, shows the approximative derivative of the upper plots. From this figure it is very clear that there is a discontinuity in the plot for the smallest FWHM.

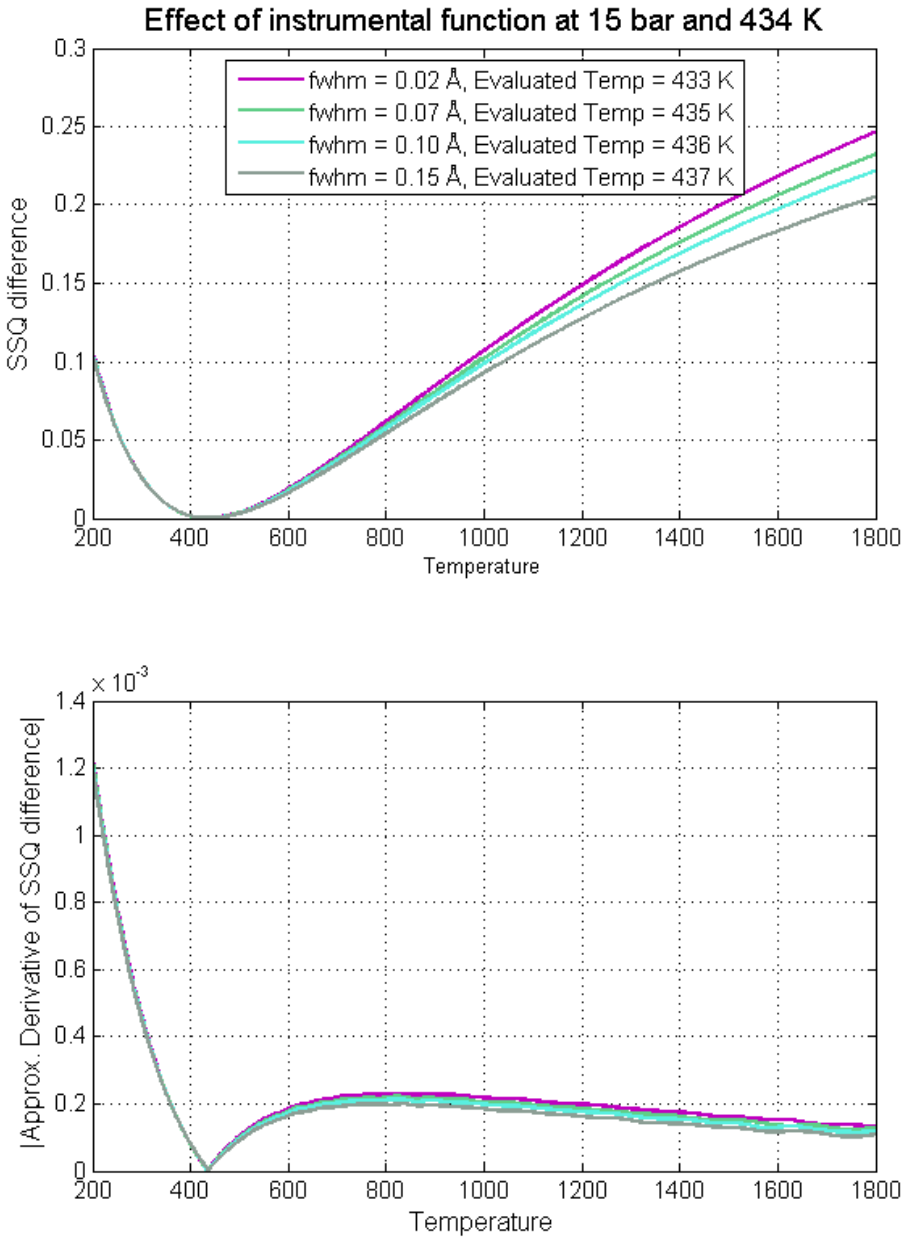


Figure 4.5: Spectra at 15 bar and 434 K evaluated with different different FWHM (0.02 Å, 0.07, 0.10, 0.15 Å) of the instrumental function. In the top panel, the SSQ-plot can be seen. The result of the minimization for each FWHM can be seen in the legend bar at the top of the diagram. The bottom panel, shows the approximative derivative of the upper plots. At this pressure there is no visible discontinuity in the plot.

## 4.2 Temperature evaluation of flame data

The LIF-measurements carried out in the flames were carried out to test the temperature evaluation on real scans at an approximative reference temperature; in this case 2200 K. The interval, 281.25-282.75 nm, were divided up into three excitation scans. A spectrum was obtained from each scan and the temperature was evaluated from it. Fig. 4.6 shows the result from the temperature evaluation in the methane/air flame. In Fig. 4.7, the corresponding spectra are compared with theoretical spectra at the evaluated temperatures. The same information for the propane/air flame can be found in Fig. 4.8 and Fig. 4.9. The evaluated temperatures for the three wavelength intervals in the flames and their mean values, can be found in Tabel 4.1. The calculated adiabatic temperatures in the both flames can be found in the last column of the table. These were calculated with a software that performs an equilibrium calculation.

Table 4.1: Evaluated mean temperature in the flames.

| | $\mathbf{T_1}$ **[K] 281.25-281.75 nm** | $\mathbf{T_2}$ **[K] 281.75-282.25 nm** | $\mathbf{T_3}$ **[K] 282.25-282.75 nm** | **<T> [K]** | $\mathbf{T_{adiab}}$ **[K]** |
|---|---|---|---|---|---|
| **Methane** | 1523 | 2233 | 2080 | 1945 | 2225 |
| **Propane** | 2075 | 2174 | 2301 | 2183 | 2284 |

The mean temperature values, <T>, are lower than the calculated adiabatic temperature, $T_{adiab}$. The evaluated temperatures from the scans across the shortest wavelengths, $T_1$, are quite low, while the temperatures of the other two scans, $T_2$ and $T_3$, are closer to $T_{adiab}$. The mean temperatures calculated without including the first scans are 2156 K for methane and 2237 for propane, which are relatively close to $T_{adiab}$. A major source of uncertainty in the evaluated temperatures is saturation. Saturated spectra would make the evaluated temperatures less accurate, since the reference spectra in the database are simulated in the linear regime. An explaination for the low values attained for the scans in the lower wavelength interval might be that the spectrum is more sensitive to saturation in that interval. As mentioned in Section 3.1.2, the laser power was not in the linear regime when performing the scans in the methane flame. The energy was lowered before the scans in the propan/air flame to decrease the saturation effects. The evaluated temperatures from the scans performed in the propane flame show smaller deviations from the adiabatic temperature than the temperature evaluated from the scans recorded in the methane flame. These results show the importance of avoiding saturation during the scans.

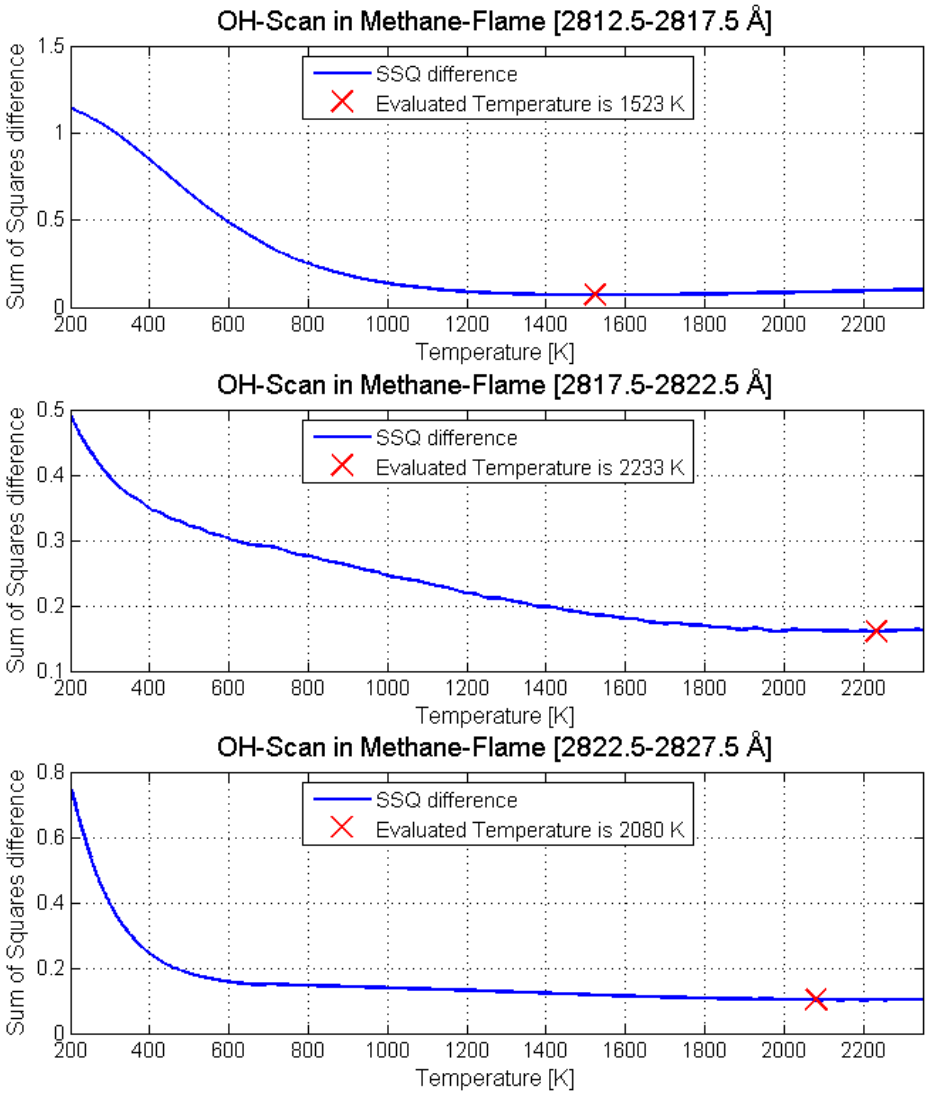


Figure 4.6: Result from temperature evaluation in the methane/air flame in the three different intervals. The SSQ-curves are minimized and the obtained temperature value is the evaluated temperature. The values are marked with a red X. The evaluted temperatures can be seen in the legend bar at the top of each plot.

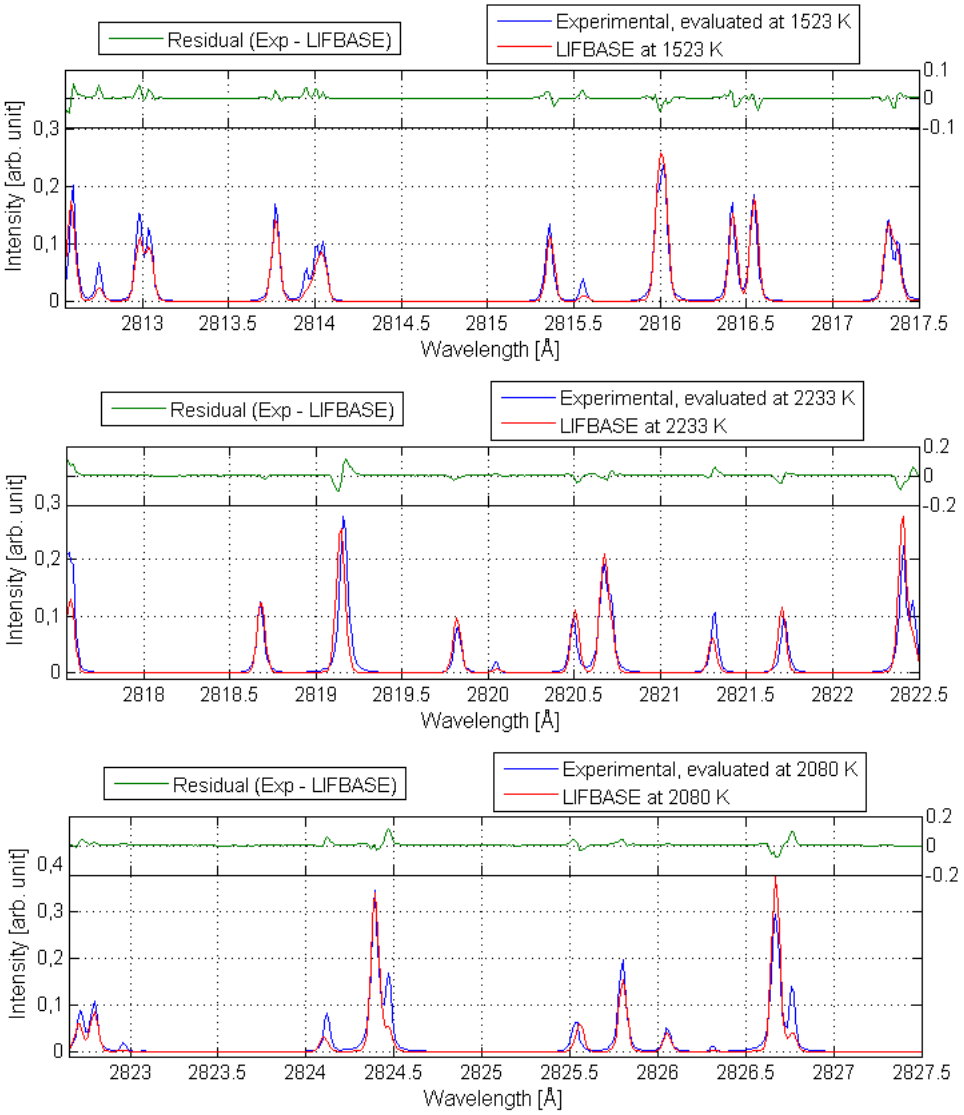


Figure 4.7: Experimental spectra from methane/air flame (blue) compared with theoretical spectra (red) at the evaluated temperature. This temperature can be seen in the legend bars. The residuals between the experimental and theoretical spectra can be seen at the top of each spectrum. The FWHM of the instrumental function was 0.045 Å.

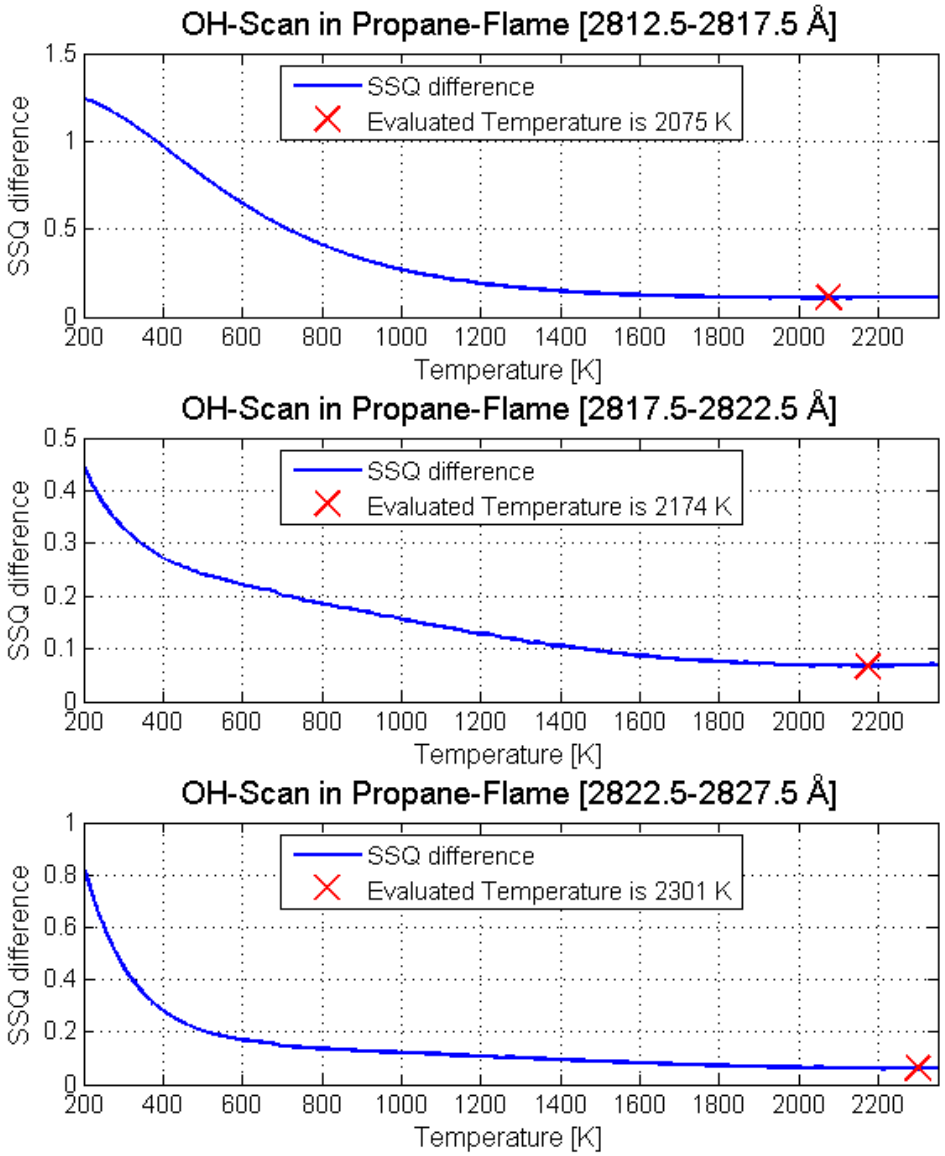


Figure 4.8: Result from temperature evaluation in the propane/air flame in the three different intervals. The SSQ-curves are minimized and the obtained temperature value is the evaluated temperature. The values are marked with a red X. The evaluted temperatures can be seen in the legend bar at the top of each plot.

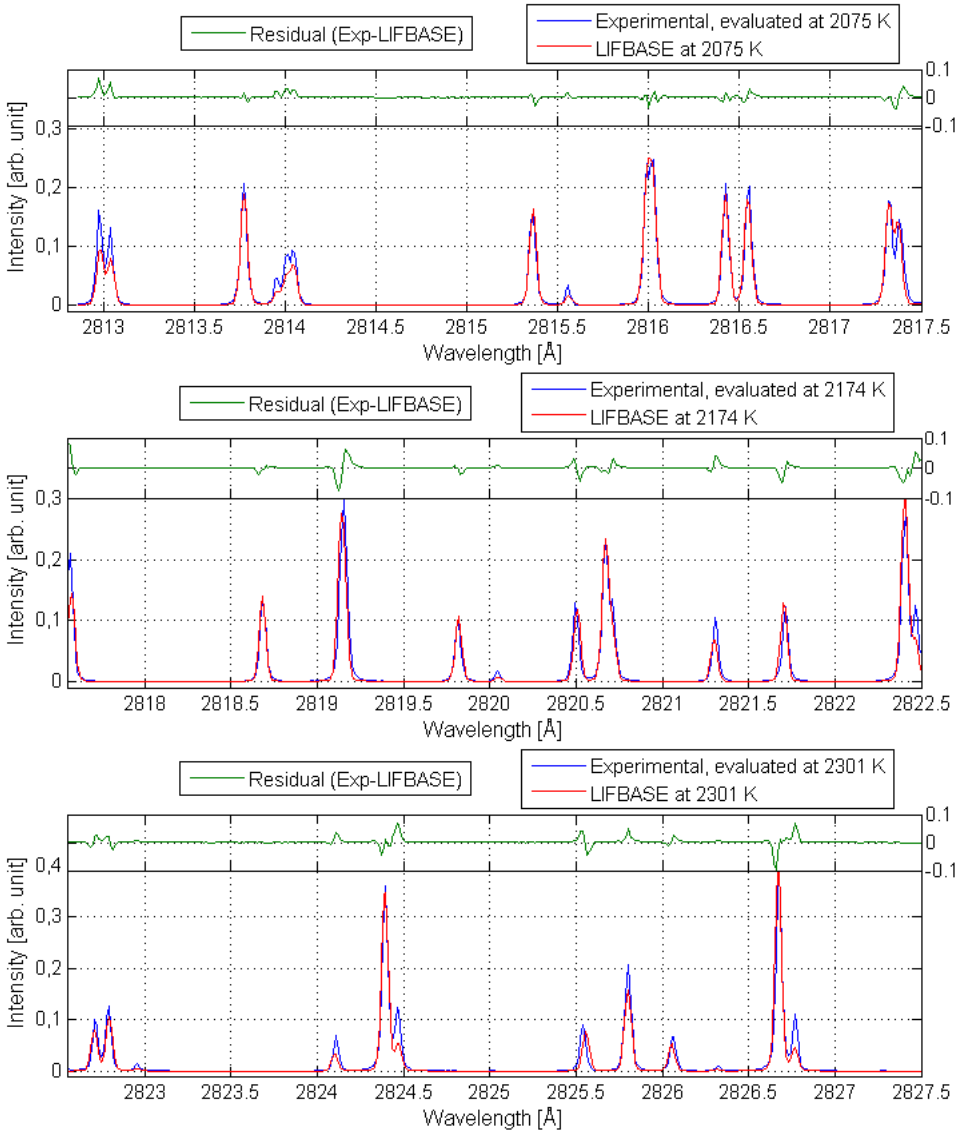


Figure 4.9: Experimental spectra from propane/air flame (blue) compared with theoretical spectra (red) at the evaluated temperature. This temperature can be seen in the legend bars. The residuals between the experimental and theoretical spectra can be seen at the top of each spectrum. The FWHM of the instrumental function was 0.035 Å.

## 4.3 Spatially resolved temperature evaluation of data acquired in $H_2O_2$-vapor

Spatially resolved temperature evaluation was initially carried out using the PF-LIF data from experiments in $H_2O_2$-vapor. In contrast to the engine measurement, the temperature of the test volume is well known (room temperature,

295 K) and it should be spatially uniform. The temperature evaluation in the x and y directions, for the two scans, can be found in Fig. 4.10 and Fig. 4.11, respectively. They are plotted with the accumulated image of the signal in the evaluated range. The mean temperature values and the standard deviations can also be seen in the two figures.

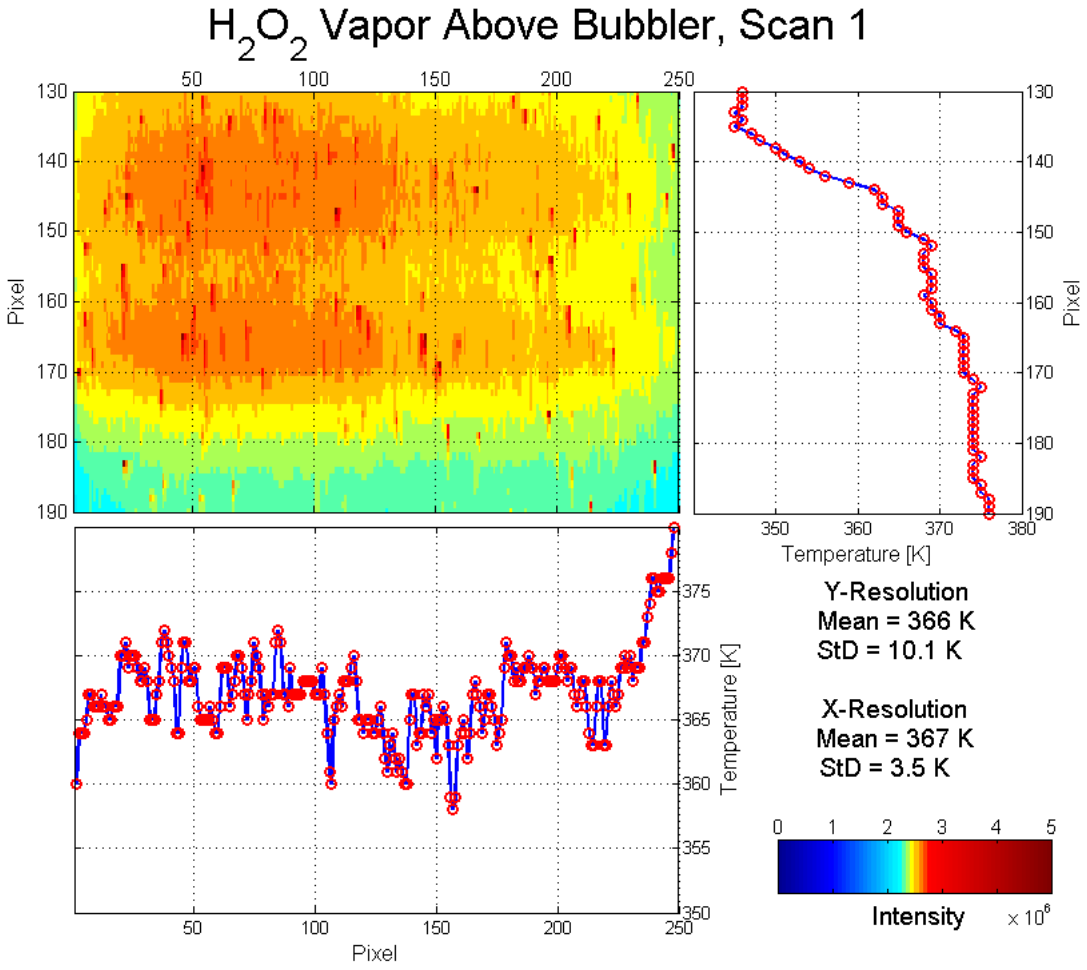


Figure 4.10: Spatially resolved temperature evaluation of the first scan in $H_2O_2$-vapor. The pulse energy was higher during this scan so there is a higher risk for saturation effects. The evaluation of a pixel row is done with a moving average where the preeceding and subsequent row are included. The image shows the intensity of the accumulated signal for the whole excitation scan.

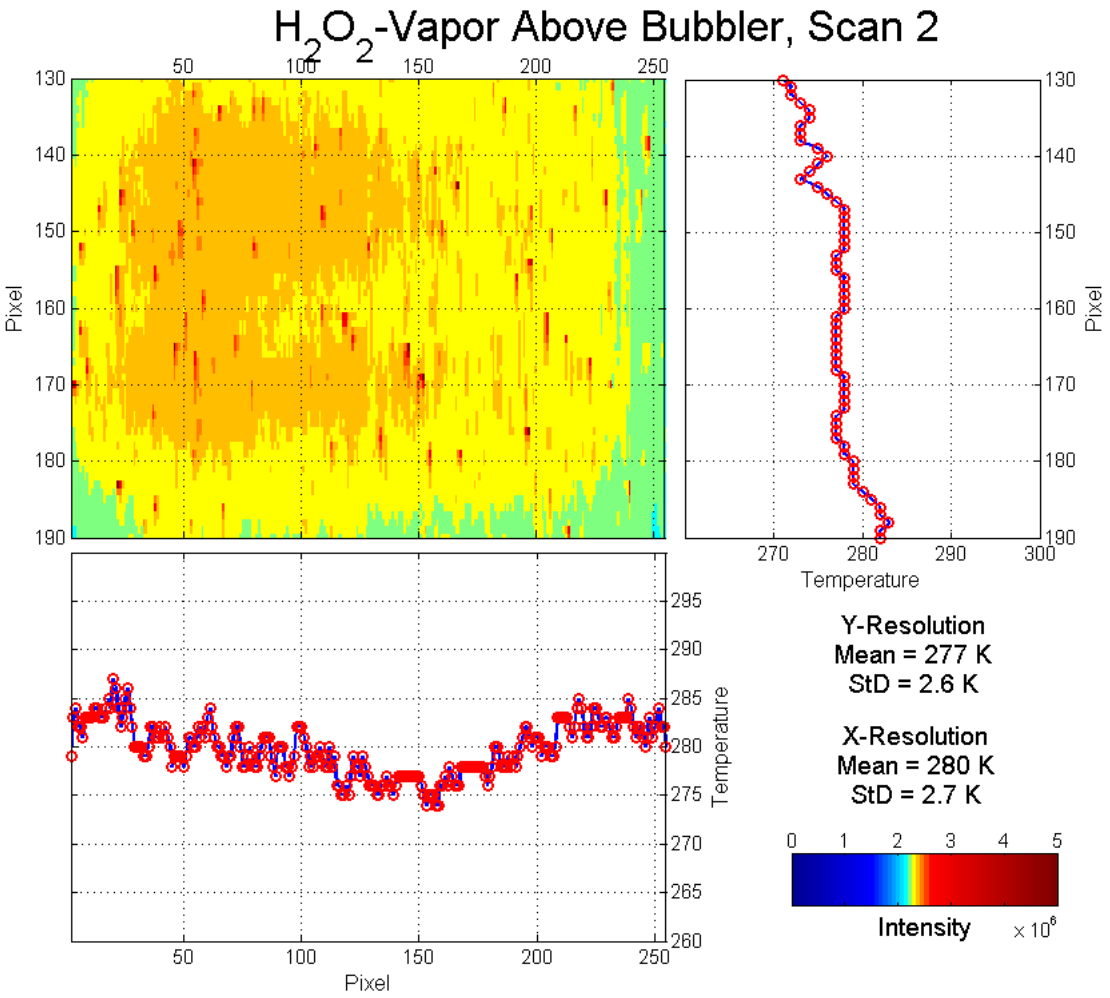


Figure 4.11: Spatially resolved temperature evaluation of the second scan in the $H_2O_2$-bubbler. The evaluation of a pixel row is done with a moving average where the previous and next row is included. The image shows the intensity of the accumulated signal for the whole excitation scan. The laser pulse energy was lower during this scan so these measurements should be closer to the linear regime.

### 4.3.1 Discussion

The evaluated mean temperature of the first scan in $H_2O_2$-vapor is around 366 K (see Fig. 4.10). The value is 60-70 K above the reference temperature of around 300 K. There is also a clear increasing temperature trend for increasing pixel rows in the y-direction. The temperature distribution should be relatively uniform and the reason for this temperature trend is unknown. The temperture distribution might not be completely homogeneous, but this would not explain a temperature change of 30 K. The most likely explaination is saturation effects due to the spatial profile of the lasers which would lead to different saturation levels in different parts of the image. Saturation would also explain why the

evaluated temperature is too high.

Before the second scan (Fig. 4.10), the laser pulse energy was lowered. The evaluated mean temperatures are closer to 300 K (around 280 K). The increasing temperature trend in the y-direction is also much smaller which indeed suggests that it is saturation effects that are causing the problems in the first scan. The obtained temperatures are actually lower than 300 K. One possible reason for this result might be uncertainty in the instrumental function used in the simulations. At 1 bar and 300 K, it would have a clear effect on the spectra and therefore on the temperature determination. Maybe a more rigorous algorithm for the determination of the instrumental function at low pressures needs to be developed. It is also important to remember that the strange "discontinuety effect" in the SSQ-curve was substantial at l bar and small FWHM of the instrumental function, since these evaluations are carried out at this pressure.

In both scans there seems to be a minimum in the evaluated temperatures around pixel row 150 in the x direction. The reason for the minimum might once again be a saturation effect since the laser sheet should have its focus at about this location. Data from the first scan also show a relatively large increase in temperature around pixel row 230 which increase the standard deviation of the mean temperature somewhat. This behavior is most likely due to lower $H_2O_2$ concentration there, since the same trend cannot be seen for the second scan. Lower concentration would mean a lower signal to noise ratio and thus a decrease in the quality of the evaluated spectra.

## 4.4 Spatially resolved temperature evaluation of HCCI-engine data

The final aim of this project was to attempt spatially resolved temperature evaluation on existing excitation scans recorded in an HCCI-engine. It was done in the x and y directions, for measurements at -13 and -23 CAD. The experimental spectra had a certain offset whose origin is not fully understood (mentioned in Section 3.2.4.1). As an attempt to deal with this offset, the evaluation was also done on the spectra after they had been adjusted. The mean values of temperature evaluation, both with and without the adjustment, can be seen in Table 4.2 and 4.3, repectively. It is difficult to judge how much an adjustment like this actually affects the results and whether the effect is the same for all the spectra. This issue, combined with the fact that the results without adjustment are closer to the calculated reference temperatures (816 K for -23 CAD and 950 for -13 CAD) and have lower standard deviations, were the basis for the decision not to do the adjustment. The spatially resolved measurements at -13 CAD and -23 CAD, without adjustment, are shown in Fig 4.13 and 4.14. The evaluated values are plotted along each axis of an accumulated image of the signal.

Table 4.2: Mean temperature of spatially resolved temperature evaluation, without adjustment

| CAD | X-Resolution | Y-Resolution | Calculated |
|---|---|---|---|
| **-13** | 979(±1.2) K | 980(±1.8) K | 950 K |
| **-23** | 867(±10.7) K | 866(±11.6) K | 816 K |

Table 4.3: Mean temperature of spatially resolved temperature evaluation, with adjustment

| CAD | X-Resolution | Y-Resolution | Calculated |
|---|---|---|---|
| **-13** | 1136(±27) K | 1142(±2.4) K | 950 K |
| **-23** | 927(±35.2) K | 937(±16.4) K | 816 K |

This evaluation has been done with an instrumental function that has a FWHM of 0.14 Å. As mentioned in Section 3.2.5, the instrumental function was chosen by manually fitting spectra to theoretical spectra in LIFBASE. Temperature evaluation (without adjustment) was done in the y-direction with instrumental functions with different FWHM and the mean temperature has been plotted in Fig. 4.12. A FWHM of 0.14 Å gives a result with the smallest standard deviation and it is closest to the calculated reference temperature.

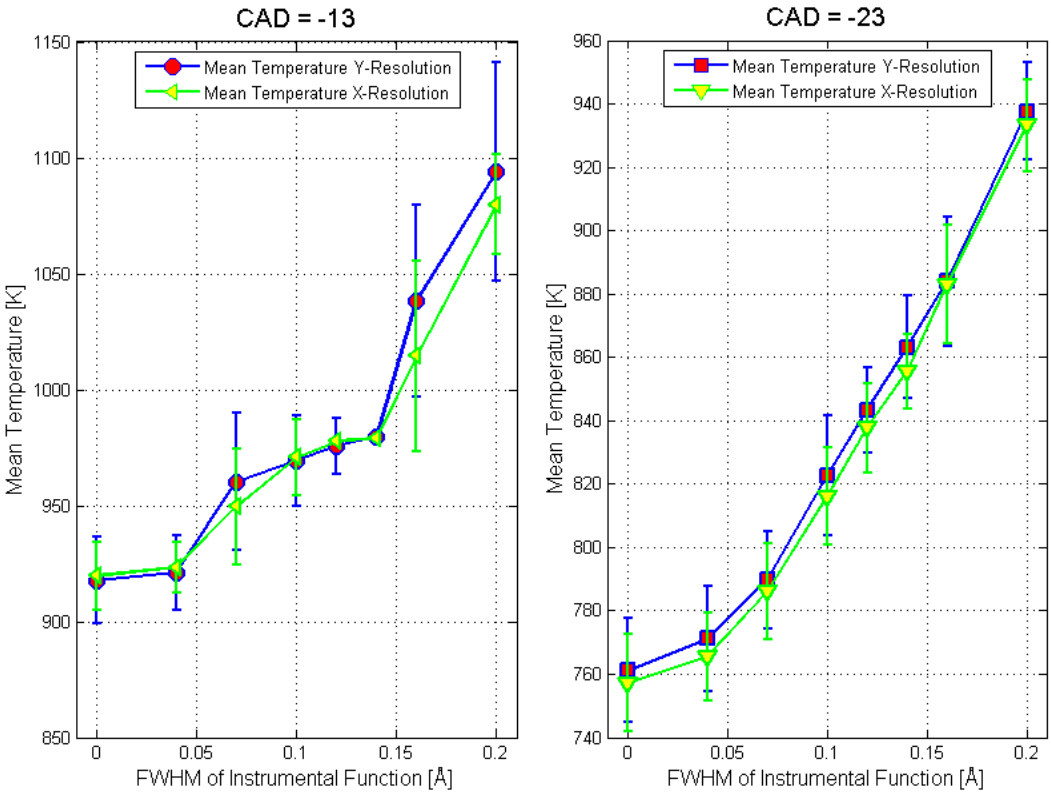


Figure 4.12: Effect of instrumental function for -13 and -23 CAD. A instrumental function with FWHM of 0.14 Å gives the smallest standard deviation and temperatures closest to the approximate references temperatures

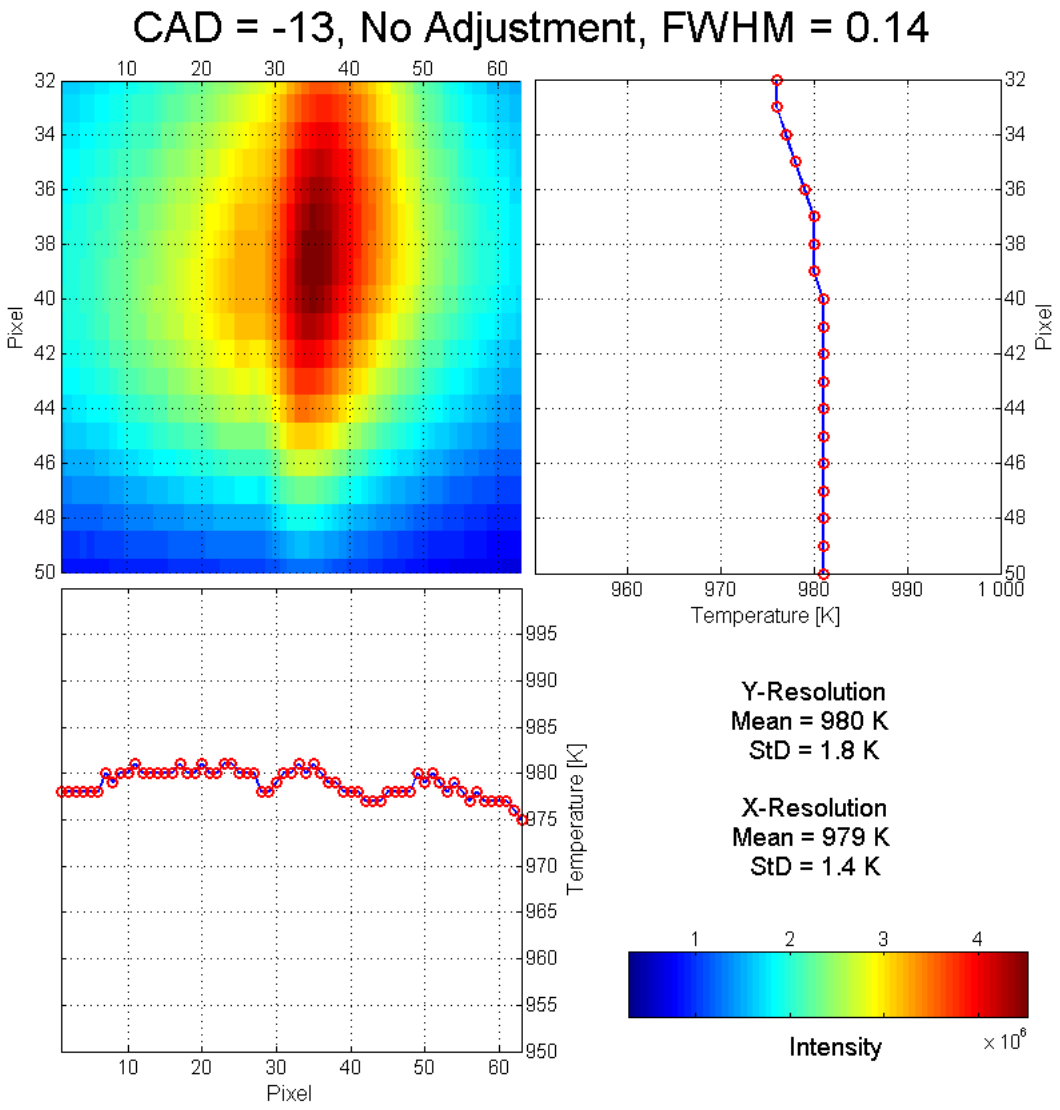


Figure 4.13: Spatially resolved temperature evaluation at each pixel row in the x-direction and y-direction, at -13 CAD. The evaluation is done for each pixel row. The image shows the intensity of the accumulated signal for the whole excitation scan.

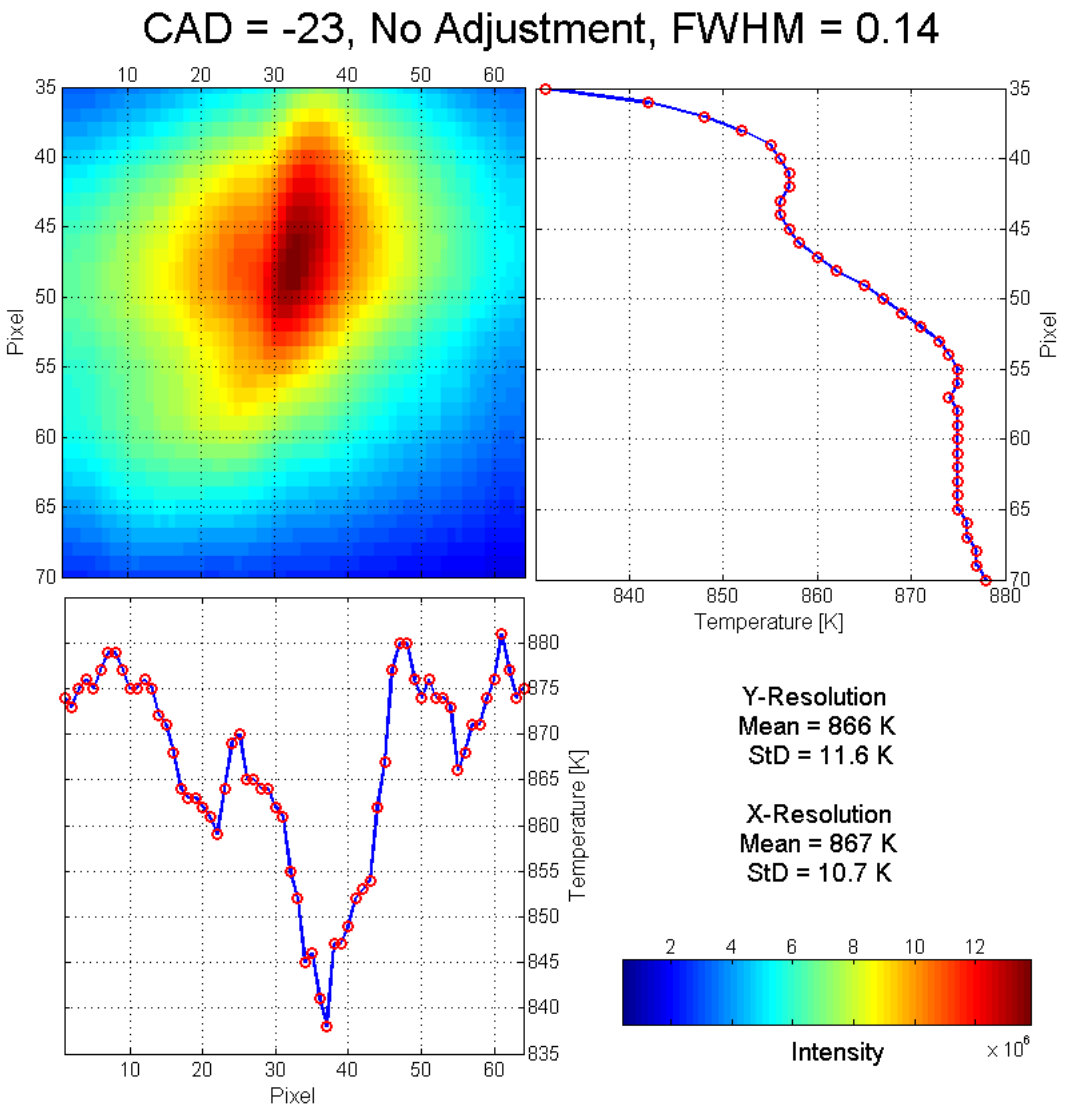


Figure 4.14: Spatially resolved temperature evaluation at each pixel row in the x-direction and y-direction, at -23 CAD. The evaluation is done for each pixel row. The image shows the intensity of the accumulated signal for the whole excitation scan.

### 4.4.1 Discussion

The evaluated mean temperature for -13 CAD is around 980 K. This value is relatively close to the calculated mean temperature of 950 K. The variations for the evaluation is small for both the x and y directions which can be seen in Fig. 4.13. The evaluation at -23 CAD, shown in Fig. 4.14, gives a mean temperature of approximately 866 K, which is around 50 K greater than the reference temperature at 816 K. The variations, and therefore the standard

deviations, at -23 CAD are also larger than at -13 CAD. Along the y-direction an increasing temperature trend can be observed with increasing pixel row. When comparing these results with the results at -13 CAD it is important to remember that the evaluated y-interval is larger at -23 CAD. Even when the size of the interval is considered the variations at -23 CAD are greater. A distinctive minimum can be seen in the temperature evaluation in the x-direction that is very similar to the one in the $H_2O_2$ scans. From Fig. 4.14 it is even more apparent that this minimum occurs at the focus of the laser sheet (between x-pixel 20 and 30) and the minimum is probably due to saturation effects. It is remarkable that there is no such minimum in the evaluation at -13 CAD despite the fact that the same laser was used.

It is hard to draw any conclusion on what is causing certain behavior in the engine since it is a turbulent and non-stationary environment. There might actually be pronounced temperature gradients in the engine. Since there were no background measurements taken for these scans there might also be unknown effects causing the difference in results both spatially and for the scans at different CAD. Some of these unknown effects might be the cause of the observed set-off mentioned earlier. Another source of error is that no compensation for laser energy variations during the scans has been done. The variations would affect the shape of the resulting spectra and consequently the temperature evaluation.

One important conclusion that can be drawn from the results, both from the $H_2O_2$-vapor and in the engine measurement, is that it is important to keep the laser pulse energy low to avoid saturation effects even though the signal to noise ratio becomes smaller.

# Chapter 5

# Conclusion

In this thesis project a method for determining spatially resolved temperatures from OH-excitation spectra has been developed. A least square algorithm was used to compare experimental spectra with theoretical spectra of known temperature. The spectra were acquired from excitation scans recorded with ICCD cameras. Temperature was evaluated from excitation scans performed in environments with well-known temperature and pressure, to test the method. These reference environments were laminar, premixed flames and $H_2O_2$-vapor. Finally, temperatures were evaluated from excitation scans recorded in an HCCI-engine.

The code is limited to evaluating OH excitation spectra, which means that it is only applicable in environments where averaging is applicable. The excitation scans in the engine were taken over many cycles and it is therefore assumed that the temperature and composition are approximately the same, at a specific CAD, for each cycle. Consequently, it is not possible to evaluate the temperature at a specific engine cycle with this technique. The spectra must also be recorded in the linear regime and be within the wavelength interval 281.0-284.6 nm. The temperature evaluation code also requires a reference mean pressure and mean temperature as input to be able to adjust the wavelength axis and estimate the instrumental function.

Non-linearity in the wavelength axis of the obtained spectra is corrected for by fitting peaks to their theoretical values. To take instrumental broadening into account, the theoretical spectra were convoluted with a Gaussian instrumental function before they were compared with the experimental spectra. The determination of instrumental function was done with a least-square algorithm for the reference scans, but had to be carried out manually for the engine scans. In the future, the instrumental function could possibly be determined with a reference excitation scan recorded with the same experimental set up, in an environment of known temperature and pressure.

The temperature evaluation of theoretical spectra showed good correlation with the theoretical temperatures. There are some issues at low pressure and small instrumental broadening. These problems could stem from numerical issues in LIFBASE or the convolution with the instrumental function. The evaluation of the spectra from the flames gave mean temperatures 100-200 K below the adiabatic temperature. A probable reason for this deviation is saturation effects. It seems like interval at lower wavelength are more sensitive to saturation effects since the evaluation of these spectra gives the temperatures

with the greatest deviation.

The developed code for spatially resolved temperature evaluation was tested on excitation scans recorded in $H_2O_2$-vapor at room temperature and atmospheric pressure. The evaluation of the first scan shows a strong temperature gradient in the y-direction. When the laser power was decreased in the second scan this gradient practically disappears. It therefore seems very likely that the gradient in the first scan is due to saturation effects. It is thus of great importance to keep the laser pulse energy as low as possible when performing excitation scans for this kind of temperature evaluation, even though the signal to noise ratio decreases.

A set-off could be observed in the spectra obtained from the engine measurements. This set-off might have something to do with the fact that no background images could be subtracted from the scans or it might possibly be some kind of saturation effect. The experimental spectra were adjusted before being compared with the theoretical spectra as an attempt to deal with this set-off. The spatial temperature evaluation was carried out with and without this adjustment. The standard deviations of the evaluated temperatures with adjustment were much larger than without. In addition, the evaluated mean temperatures were further from the calculated mean temperatures. It was therefore decided not to do the adjustment.

The results from the engine measurements give mean temperatures fairly close to the calculated reference temperatures. They are about 30-60 K higher. The spatially resolved temperatures at -13 CAD in the HCCI-engine have very small variations in both the x and y direction, while the standard deviations are about ten times greater at -23 CAD. It is hard to determine the reasons for the difference since there are so many unknown factors in the engine measurements. To further investigate the reasons, new excitation scans specifically performed for temperature evaluation should be carried out at different CADs in an engine.

## 5.1 Future Outlook

The evaluation method has only been used on reference spectra at one high temperature, 2200 K, and one low temperature, 300 K, but not for any known temperatures in between. A possible future task would be to carry out excitation scans with PF-LIF on $H_2O_2$-vapor, heated to different temperatures, and thereby acquire spectra in a larger temperature range. New scans, specifically done for temperature evaluation, should also be performed in an HCCI engine. A desirable future prospect would be to be able to perform temperature evaluation close to surfaces (walls or piston) in the engine and study the nature of the temperature gradients which theory states should be there.

During all the new exciation scans, the laser pulse energy should be kept as low as possible to avoid saturation effects. The laser pulse energy should also be monitored to be able to compensate for the change in the gain of the laser dye during the scans. Proper background measurements should also be undertaken. To determine the instrumental function, reference excitation spectra at known temperature and atmospheric pressure should be acquired with the experimental setup. The laser spectral profile, could perhaps also be measured to get more accurate information about the profile of the instrumental function.

The code should be cleaned up and optimized to perform faster and possibly

be made more general. The grid for the theoretical temperatures and pressures in the database could be reduced to see if this would improve the temperature evaluation. Another future outlook would be to create a full two-dimensional temperature map by evaluating temperatures in each pixel or cluster of pixels, and not just in pixel rows. LIFBASE is a powerful software but the odd issue, causing the "discontinuety" in the sum of square plots should be investigated further. It is also possible that there are some uncertainties in the calculated collisional broadening in LIFBASE at higher pressures since the data used to determine the constants in the empirical expression were acquired at low pressure (1-10 bar). It would be useful to investigate the extent of these uncertainties.

One possible way of making the temperature determination more efficient and accurate could be to identify certain parts or peaks of the OH-spectrum providing higher temperature sensitivity. If only specific parts of the spectra were used, the excitation scans would be shorter and the measurement time would decrease. The ideal situation would be a single shot method that could be used for online temperature determination. A potential way of doing this is a two-line concept, where the ratio of two temperature sensitive peaks is the parameter used when comparing experimental and theoretical spectra. A technique like this would not require excitation scans. Two synchronized probe lasers would instead be tuned to one peak each and the corresponding emitted fluorescence would be measured. There would be an intensity ratio for each time the two lasers are fired which could be used for online temperature evaluation. With a technique like this, the temperature at a specific CAD in a specific engine cycle could be determined, even in two dimensions. Such a measurement tool would supply researchers with extremely important experimental data for validation of combustion models.

# Appendix A

# Hund's Coupling Cases

Hund's cases are coupling schemes in spectroscopy of diatomic molecules. They are idealized cases where a specific coupling between angular momenta is said to dominate. In Hund's case (a) the electron orbital angular momentum, L, is coupled to the internuclear axis and spin-orbit interaction couples the electronic spin, S, to L. In the vector model (see Fig. A.1) this means that L and S precess around the internuclear axis. They have both well-defined projections on the internuclear axis, $\Lambda$ and $\Sigma$. These couple and form the vector, $\Omega$. $\Omega$ and the rotational angular momentum of the nuclei, R, form the total angular momentum, J. In case (a), the precession of S around the internuclear axis is much faster than the rotational velocity of the molecule. When J increases this will not be the case anymore. In Hund's case(b) the spin will uncouple from the internuclear axis and the spin-orbit interaction between L and S will be weak. $\Omega$ will no longer be well-defined. Instead $\Lambda$ and R forms the vector N, and N and S couple to form J.

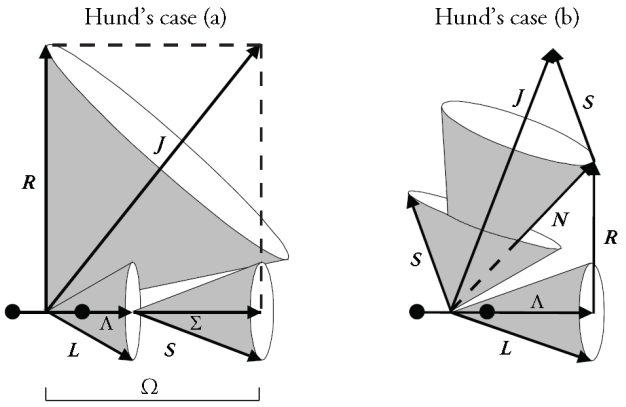


Figure A.1: Hund's coupling case (a) and (b).

# Appendix B

# MATLAB-code

## Temperature Evaluation on Engine Scans

Spatially resolved temperature evaluation at -13 or -23 CAD in the HCCI-engine . The evaluation is done by fitting experimental spectra with theoretical spectra with a least square algorithm. Here the spatial resolution is in the x direction. The functions readMotorSpecX, FixXScale and peaks can be found further down. The code evaluating temperature in the $H_2O_2$-vapor and the flames is very similar to this code. The main different is that the change in laser pulse energy is compensated for. The instrumental function is also calculated with the same least square algorithm used here. For further information on the code, please contact author.

```
CAD = input('CAD [23 eller 13]?: ');
if CAD == 23
    ymin = 35;
    ymax = 70;
    xmin = 1;
    xmax = 64;
    pRef = 15;      %Reference Pressure
    pExp = pRef;
    tempRef = 800;
    fwhm = 0.14;     % Full Width Half Max
elseif CAD == 13
    ymin = 30;
    ymax = 50;
    xmin = 1;
    xmax = 63;
    pRef = 22;      % Reference Pressure
    pExp = pRef;
    tempRef = 950;  % Reference Temperature
    fwhm = 0.14;    % Full Width Half Max
end

i = -CAD;
```

```
if i == -23
    RefSpec = readMotorSpecX(i,2,60,30,70); % Acquire reference spectra
elseif i == -13
    RefSpec = readMotorSpecX(i,2,60,30,50); % Acquire reference spectra
end
% Calculate X-axis adjustment
[RefSpec,poly] = FixXscale(RefSpec,pRef,tempRef);
```

### Spacial resolution

```
MinTemp=[];
for j = xmin:1:xmax

    % Experimental data
    ExpSpec = readMotorSpecX(i,j,j,ymin,ymax);
    % Correct X-Axis
    CorrectedXAxis = feval(poly,ExpSpec(:,1));
    ExpSpec(:,1) = CorrectedXAxis;
    % Normalize
    ExpSpecNorm = normc(ExpSpec(:,2));
```

### Least Square Method.

```
    TempArray = 200:25:1800; % Temperatures
    Error = double.empty(1,length(TempArray),0);
    position = 1;
    TempIndex = 0;
    for t = TempArray
            stringName = [num2str(pExp) 'bar' num2str(t) 'K.txt'];
            % Get LIF-spectra at temperature t.
            LifSpec = importdata(stringName);
            LifSpec = LifSpec(:,1:2:end);
            % Convolution with instrument function.
            if fwhm > 0
                LifSpec = falt(LifSpec,fwhm);
            end
            % Fit and cubic interpolation of LifSpec
            LifSpecFit = fit(LifSpec(:,1),LifSpec(:,2),'cubicinterp');
            LifSpecNew = feval(LifSpecFit,ExpSpec(:,1));
            % Normalize
            LifSpecNorm = normc(LifSpecNew);
            % Sum of Squares Error
            error = sum((ExpSpecNorm-LifSpecNorm).^2);
            Error(1,position,1) = error;
            position = position + 1;
    end
    % Fit and interpolation of Sum of Squares Error
    TFit  = fit(TempArray',Error','cubicinterp');
    Temperatures = 200:max(TempArray);
    TempFit = feval(TFit,Temperatures);
```

```
    % Find Minimum
    [err, tempIndex] = min(TempFit);
    T = Temperatures(tempIndex);
    MinTemp = [MinTemp T];

end
TempMean = mean(MinTemp);    % Mean temperature of spatially resolved temperature eval.
TempStd = std(MinTemp);      % Standard Deviation
```

### Plot result

```
figure(1)
plot(xmin:xmax,MinTemp,'-','LineWidth',2)
hold on
plot(xmin:xmax,MinTemp,'Or','LineWidth',2)
xlabel('Pixel')
ylabel('Temperature [K]')
grid on
xlim([xmin xmax])
title(['CAD=' num2str(i) ', fwhm=' num2str(fwhm) ',Mean=' num2str(TempMean)
       ' K, STD=' num2str(TempStd) ' K'])
```

## ReadMotorSpecX

Creates a spectrum from the intensity values in x-pixel 'start' to 'stop' and y pixel 'ymin' to 'ymax' dor the chosen CAD.

```
function [MotorSpec] = readMotorSpecX(CAD,start,stop,ymin,ymax)

if CAD == -23
    numOfImages = 2200;
    values = zeros(numOfImages-1,1);
    index = 1:numOfImages-1;

    % OH-scan
    for i = index
    im = readspe('scan_minus23CAD.SPE',i);
    background = mean2(im(95:100,:));
    finalImage = im-background;
    finalImage = finalImage(ymin:ymax,start:stop);
    values(i) = sum(sum(finalImage));
    end
    values = values(30:end-160); % Remove edges of spectrum
    % normalize
    valuesNorm= normc(values);
    % Ångström-scale
    xAxis =linspace(2811.08,2831.2,2010);
    % Save Spectrum
    MotorSpec= [xAxis' valuesNorm];
```

```
elseif  CAD == -13

    numOfImages = 2200;
    values = zeros(numOfImages-1,1);
    index = 1:numOfImages-1;

    % OH-scan
    for i = index
    im = readspe('scan_minus13CAD.SPE',i);
    background = mean2(im(95:100,:));
    finalImage = im-background;
    finalImage = finalImage(ymin:ymax,start:stop);
    values(i) = sum(sum(finalImage));
    end
    values = values(30:end-160); % Remove edges of spectrum
    % normalize
    valuesNorm= normc(values);
    % Ångström-scale
    xAxis =linspace(2811.08,2831.2,2010);
    % Save Spectrum
    MotorSpec= [xAxis' valuesNorm];
else
    disp('No data at that CAD') % Wrong CAD
    MotorSpec = 1;
end
end
```

## FixXScale

Corrects the wavelength axis of EXP by finding and fitting peaks with theoretical values at pressure P and temperature T.

```
function [CorrectedSpectrum, p] = FixXscale(EXP,P,T)

Positions = [2810.9 2812.1 2813.1 2816:2819 2821 2822 2823 2824 2826 2827
             2829 2831 2832 2834 2835 2837 2839 2841 2845];
Reference = importdata([num2str(P) 'bar' num2str(T) 'K.txt']);
Reference=Reference(:,1:2:3);

% Find peaks in Reference.
[locs_ref,pks_ref,Positions] = peaks(Reference,Positions,0.49,0.49);
 LinePositions = locs_ref;

% Make sure the spectrum is in the right interval
if EXP(end,1) < LinePositions(1) || EXP(1,1) > LinePositions(end)
    error('Fel intervall på spektrum')
end
% Remove theoretical linepositions outside of the spectrums interval (high)
```

```
for i = 2:length(LinePositions)
    if EXP(end-10,1)< LinePositions(i)
        LinePositions = LinePositions(1:i-1);
        break
    end
end
% Remove theoretical linepositions outside of the spectrums interval (low)
for i = 1:length(LinePositions)
    if EXP(10,1)< LinePositions(i)
        LinePositions = LinePositions(i:end);
        break
    end
end

% Find peaks in EXP
EXP(:,2) = 100*EXP(:,2)/max(EXP(:,2));
[pos_exp,pks_exp,LinePositions] = peaks([EXP(:,1) EXP(:,2)],LinePositions,0.17,0.17);
% Fit
p =fit(pos_exp',LinePositions','linearinterp');
CorrectedXAxis = feval(p,EXP(:,1));
CorrectedSpectrum =[CorrectedXAxis normc(EXP(:,2))];
```

## peaks

Finds the tallest peak in interval around the positions in LinePositions. and saves the position in POS.

```
function [POS,PKS,A] = peaks(EXP, LinePositions, a, b)

if nargin == 2
    a = 0.1;
    b =a;
end
LOCS=[];
POS=[];
PKS=[];
interval = [];
% Create interval (-a +b) to look for peak
for i = 1:length(LinePositions)
    xmin = LinePositions(i)- a;
    xmax = LinePositions(i)+ b;
    interval = [interval; xmin xmax];
end
% Make sure interval is in spectrums interval
if interval(1,1) < min(EXP(:,1))
        interval(1,1) = min(EXP(:,1));
end
if interval(end,end) > max(EXP(:,1))
        interval(end,end) = max(EXP(:,1));
```

```
end
% Find peaks in interval
Remove = [];
for i = 1:length(interval(:,1))
    xMin=find(EXP(:,1)<= interval(i,1));
    xMax=find(EXP(:,1)>= interval(i,2));
    EXP_new = EXP(xMin(end):xMax(1),1);
    [pks,locs]=findpeaks(EXP(xMin(end):xMax(1),2),'sortstr','descend','minpeakheight',0.2)
    if length(locs) < 1
        Remove = [Remove i];
        continue
    end
    %Save the tallest peak
    POS = [POS EXP_new(locs(1))'];
    PKS = [PKS pks(1)'];
end
LinePositions(Remove) = []; % Remove peaks not found
A = LinePositions;
```

# Bibliography


[1] S. R. Turns. *An introduction to Combustion: Concepts and Applications*. McGraw-Hill Book Co, 2nd edition, 200.

[2] J. Kiefer, A. Meyerhoefer, T. Seeger, A. Leipertz, Z.S. Li, and M. Aldén. OH-thermometry using laser polarization spectroscopy and laser-induced fluorescence spectroscopy in the OH A-X (1,0) band. *Journal of Raman Spectroscopy*, 40(7):828–835, 2009.

[3] C. Copeland, J. Friedman, and M. Renksizbulut. Planar temperature imaging using thermally assisted laser induced fluorescence of OH in a methane/air flame. *Experimental Thermal and Fluid Science*, 31(3):221 – 236, 2007.

[4] MATLAB. version 8.0 (r2012b), 2012.

[5] A. C. Eckbreth. *Laser Diagnostics for Combustion Temperature and Species*. Gordon and Breach Publishers, 2 edition, 1996.

[6] J. Luque and D.R. Crosley. Lifbase: Database and spectral simulation program (version 2.1.1). SRI International Report MP 99-009, 1999.

[7] L. Martinsson, P.-E. Bengtsson, M. Aldén, S. Kröll, and J. Bonamy. A test of different rotational raman linewidth models: Accuracy of rotational coherent anti-stokes raman scattering thermometry in nitrogen from 295 to 1850 K. *The Journal of Chemical Physics*, 99(4):2466–2477, 1993.

[8] Wolfgang G. Bessler, Christof Schulz, Volker Sick, and John W. Daily. A versatile modeling tool for nitric oxide LIF spectra. *Proceedings of the Third Joint Meeting of the U.S. Sections of The Combustion Institute (Chicago, March 16-19, 2003, paper PI05)*, March 2003.

[9] B. Li, M. Jonsson, M. Algotsson, J. Bood, Z.S. Li, O. Johansson, M. Aldén, M. Tunér, and B. Johansson. Quantitative detection of hydrogen peroxide in an HCCI engine using photofragmentation laser-induced fluorescence. *Proceedings of the Combustion Institute*, 34(2):3573 – 3581, 2013.

[10] S Svanberg. *Atomic and Molecular Spectroscopy: Basic Aspects and Practical Applications*. Springer, 3 edition, 2001.

[11] G. Blom, J. Enger, G. Englund, J.Grandell, and L. Holst. *Sannolikhetsteori och statistikteori med tillämpningar*. Studentlitterature, 2005.

[12] Jie-Li Lin, Yu-Yan Liu, Hong-Ping Liu, Yuan-Qing Quo, Xiao-Yong Liu, Feng-Yan Li, and Jin-Rui Li. Measurement of pressure-broadening linewidths of no from the fitting of LMR spectra with corrections of instrumental broadening. *Modern Physics Letters B*, 14(11):401, 2000.

[13] Igor M. Sokolov Werner Eberling. *Statistical Thermodynamics and Stochastic Theory of Nonequilibrium Systems*. World Scientific Publishing Co. Pte. Ltd., 2005.

[14] Billy Kaldvee. *Development and application of single-ended picosecond laser diagnostics*. PhD thesis, Lund University, 2012.

[15] F. Reif. *Fundamentals of Statistical and Thermal Physics*. McGraw-Hill Book Co, 1965.

[16] O. Johansson. *Development and Application of Photofragmentation Laser-Induced Fluorescence for Visualization of Hydrogen Peroxide*. PhD thesis, Lund University, 2011.

[17] C. N. Banwell and E. M. McCash. *Fundamentals of molecular spectroscopy*. McGraw-Hill, 1994.

[18] U. E. Meier, D. Wolff-Gassmann, and W. Stricker. LIF imaging and 2d temperature mapping in a model combustor at elevated pressure. *Aerospace Science and Technology*, 4(6):403 – 414, 2000.

[19] Z.S. Li, B. Li, Z.W. Sun, X.S. Bai, and M. Aldén. Turbulence and combustion interaction: High resolution local flame front structure visualization using simultaneous single-shot PLIF imaging of CH, OH, and $CH_2O$ in a piloted premixed jet flame. *Combustion and Flame*, 157(6):1087 – 1096, 2010.

[20] U. Brackmann. *Lambdachrome Laser Dyes*. Lambda Physik, 1997.

[21] O. Johansson, J Bood, M. Aldén, and U. Lindblad. Hydroxyl radical consumption following photolysis of vapor-phase hydrogen peroxide at 266 nm: Implications for photofragmentation laser-induced fluorescence measurements of hydrogen peroxide. *Applied Physics B: Lasers and Optics*, 97(2):515–522, 2009.

[22] E.C. Rea Jr., A.Y. Chang, and R.K. Hanson. Shock-tube study of pressure broadening of the $A^2\Sigma^+ - X^2\Pi(0,0)$ band of OH by Ar and $N_2$. *Journal of Quantitative Spectroscopy and Radiative Transfer*, 37(2):117–127, 1987.

[23] K. Kohse-Höinghaus, U. Meier, and B. Attal-Trétout. Laser-induced fluorescence study of OH in flat flames of 1-10 bar compared with resonance CARS experiments. *Applied Optics*, Vol. 29 Issue: 10 p:p1560–1569, 10p, 1990.